

Article

Initial Accretion in Hamelin Pool Microbialites: The Role of *Entophysalis* in Precipitation of Microbial Micrite

Brooke E. Vitek ¹, Erica P. Suosaari ^{2,3,*}, John F. Stolz ⁴ , Amanda M. Oehlert ¹  and R. Pamela Reid ¹ ¹ Rosenstiel School of Marine and Atmospheric Science, University of Miami, Miami, FL 33149, USA² Department of Mineral Sciences, National Museum of Natural History, Smithsonian Institution, Washington, DC 20560, USA³ Bush Heritage Australia, 395 Collins St., Melbourne, VIC 3000, Australia⁴ Department of Biological Sciences, Duquesne University, Pittsburgh, PA 15282, USA

* Correspondence: suosaarie@si.edu

Abstract: One of the largest assemblages of living marine microbialites, with shapes and sizes analogous to ancient structures, is found along the margins of Hamelin Pool, Shark Bay, Western Australia. An investigation of microbial mats on the surfaces of these structures using petrographic analysis, light, and scanning electron microscopy identified the in situ precipitation of micrite as an important accretion mechanism in all major mat types (pustular, smooth, and colloform). Within each mat type, peloidal micrite, composed of nano-bulbous spheres to tabular and rod-shaped crystals, was closely linked with cells of the coccoid cyanobacterium *Entophysalis*, and microtextures of the micrite reflected the size and distribution of *Entophysalis* colonies. In pustular surface mats, where large colonies of *Entophysalis* were common, large clots of micrite were distributed randomly throughout the mat. In contrast, in smooth and colloform mats, where smaller colonies of *Entophysalis* were distributed along horizons, micrite formed fine laminae. In all surface mat types, micrite associated with *Entophysalis* had a characteristic honeycomb appearance, resulting from cell and/or colony entombment. These findings redefine our understanding of microbialite accretion in Hamelin Pool, recognizing the importance of microbial micrite in microbialite growth and showing that coccoid cyanobacteria are capable of building laminated structures. Moreover, *Entophysalis*, the dominant visible microbe associated with the precipitation of micrite in Hamelin Pool, has a lineage to *Eoentophysalis*, found throughout early and middle Proterozoic microbialites assemblages. These findings reinforce the importance of Hamelin Pool as a window to the past.



Citation: Vitek, B.E.; Suosaari, E.P.; Stolz, J.F.; Oehlert, A.M.; Reid, R.P. Initial Accretion in Hamelin Pool Microbialites: The Role of *Entophysalis* in Precipitation of Microbial Micrite. *Geosciences* **2022**, *12*, 304. <https://doi.org/10.3390/geosciences12080304>

Academic Editors:
Jesus Martinez-Frias and
Christophe Thomazo

Received: 17 June 2022
Accepted: 5 August 2022
Published: 9 August 2022

Publisher's Note: MDPI stays neutral with regard to jurisdictional claims in published maps and institutional affiliations.



Copyright: © 2022 by the authors. Licensee MDPI, Basel, Switzerland. This article is an open access article distributed under the terms and conditions of the Creative Commons Attribution (CC BY) license (<https://creativecommons.org/licenses/by/4.0/>).

Keywords: microbialite; *Entophysalis*; micrite; Hamelin Pool; Shark Bay; stromatolite

1. Introduction

The earliest macroscopic evidence of life on Earth is found in the form of microbialites, organosedimentary structures built by benthic microbial communities [1]. These ancient sedimentary structures have persisted on Earth for the past 3.5 billion years and can still be found growing in several locations around the world today. Microbialites of the Proterozoic were diverse in morphology and are credited with oxygenating Earth's early atmosphere [2]. Until the Cambrian, microbialites are believed to have dominated shallow marine environments [3]. Today, one of the world's most extensive and diverse living microbialite systems is found along the shorelines of Hamelin Pool in Shark Bay, Western Australia (Figure 1).

Microbialite accretion occurs by two dominant processes: trapping and binding of detrital grains and in-situ precipitation of microcrystalline calcium carbonate (<4 µm) [1,4], hereafter referred to as micrite. Detrital grains are trapped and bound by microbes and associated extracellular polymeric substances (EPS) [5,6]. Micrite in microbialites is typically considered to be precipitated in situ via localized geochemical changes [5,7–9], but also could be detrital, i.e., fine sediment grains from the local environment that are trapped

and bound by a microbial mat [5]. The in situ precipitation of micrite can be a result of inorganic geochemical processes or can be biologically induced [10].

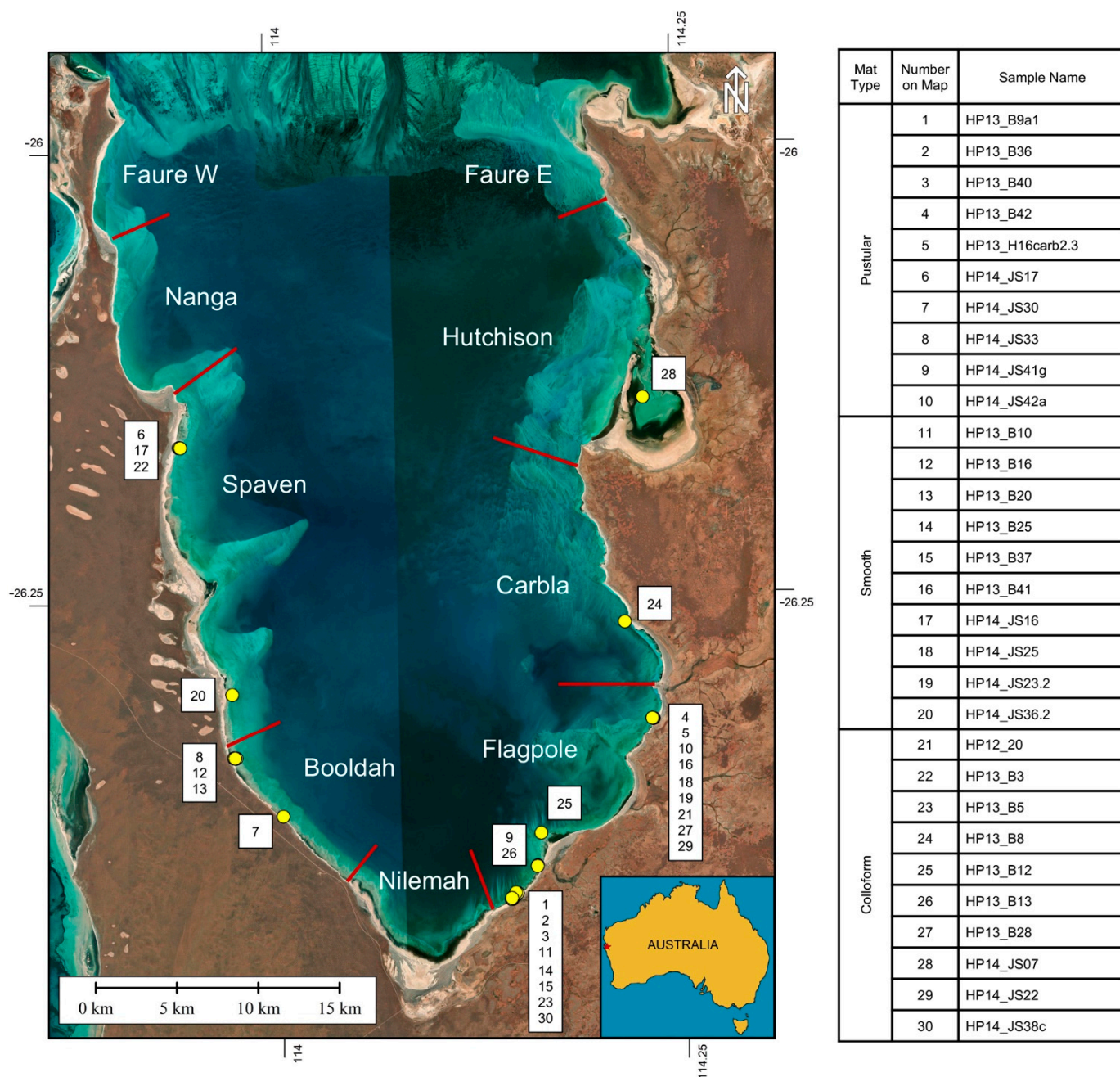


Figure 1. Location map showing Hamelin Pool in Shark Bay, Western Australia, with Stromatolite/Microbialite Provinces described by [11,12]. Numbered yellow dots indicate the locations of samples used for petrographic analysis to estimate the abundance of micrite versus grains in surface mats. Mat types and sample names corresponding to the numbered locations are indicated in the table; additional details are provided in Supplemental Table S1. Base map: SIO, NOAA, US Navy, NGA, GEBCO, Image Landsat/Copernicus.

Ancient microbialites are mainly micritic, lacking sand-sized components [13,14]. Previous authors have argued that modern marine microbialites differ from ancient counterparts due to the dominance of sand grains and relative paucity of micrite observed in the modern structures [15,16]. However, recent studies have reported an abundance of micrite in several fabrics forming Hamelin Pool microbialites [6,11,17,18]. Here, we

document in situ micrite precipitation in Hamelin Pool microbialites, using thin section petrography, light microscopy, and scanning electron microscopy (SEM) with an energy dispersive X-ray spectrometer (EDS). We focus on micrite associated with initial accretion by microbialite-forming surface mats, thereby addressing the following questions: What are the amounts and distribution of micrite in surface mats of Hamelin Pool microbialites? What is the origin of the micrite? And, do microbes influence the micritic textures? The results redefine our understanding of initial accretion in the surface mats of Hamelin Pool microbialites and highlight the value of this system as a modern analog for interpreting fossil microbialites.

2. Background: Microbialite-Forming Microbial Mats in Hamelin Pool

Hamelin Pool, located in Shark Bay, Western Australia (Figure 1), is home to one of the largest living assemblages of modern stromatolites with sizes and shapes equivalent to Precambrian forms. Dominating nearly the entire 135 km of Hamelin Pool's coastline, these microbialites have commonly been considered modern analogs for fossil structures [19–22] since their discovery in the 1950s [23].

Three types of microbialite-forming mats are recognized in Hamelin Pool: pustular, smooth, and colloform (Figure 2) [11,23–25]. The growth model proposed by Suosaari et al., [11] (Figure 3) differs from previous models e.g., [17,25], as it differentiates smooth and pustular mats that form “poorly lithified sheets” in upper intertidal zones from smooth and pustular mats forming “discrete lithified structures” in lower intertidal and subtidal zones. Light microscopy indicates that the pustular sheet mats are dominated by *Entophysalis major* with some *E. granulosa*, whereas pustular mats forming lithified buildups have a more diverse community that includes *Dicothrix* and *Scytonema* in addition to *Entophysalis* species [11]. Smooth mats forming sheets are dominated by the filamentous cyanobacteria *Microcoleus* and *Schizothrix*, whereas smooth mats forming lithified buildups are dominated by coccoid cyanobacteria *Aphanothece*, *Aphanocapsa*, and *Entophysalis*, and diatoms [11]. Colloform mats are similar in composition to smooth mats, dominated by *Aphanothece*, *Aphanocapsa*, and *Entophysalis*, and diatoms [11]. Recent metagenome studies of smooth and colloform mats showed few taxonomic and functional gene differences between the two mats, indicating that the differences in surface morphology are likely a reflection of environmental pressures [26]. Note that the genus *Entophysalis* is not identified in molecular studies [26] because 16S rRNA sequences are not currently available due to a lack of axenic cultures.

Unrecognized in early descriptions of microbialite-forming mats in Hamelin Pool e.g., [23–25], the coccoid cyanobacterium *Entophysalis* is a significant component of all three structure-building mats: pustular, smooth, and colloform mats [11]. *Entophysalis* is one of the oldest recognized coccoid microbialite-forming cyanobacteria, with a lineage that extends back to the mid-Precambrian [27]. *Entophysalis* is comprised of coccoid colonial unicells (Figure 4A,B) that reproduce by cell division in three planes, forming cell aggregates [27]. With each subsequent cell division, a new gelatinous envelope is produced around the cells within the original envelope (Figure 4C). This results in a series of encapsulating envelopes, the number of which increases with the age of the colony. These envelopes are composed mainly of hydrated polysaccharides and tangentially-oriented ultrafine fibers; the envelopes expand and contract due to hydration or water loss during subaerial exposure [28]. The mineralization of cell envelopes has previously been described in pustular mats from Hamelin Pool by Golubic and Hofmann [27]. In this paper, we show that micrite precipitated in association with *Entophysalis* is an important accretion mechanism within all three surface mat types from Hamelin Pool stromatolites. Indeed, microbialite growth in Hamelin Pool is primarily an *Entophysalis* story that provides important insight into microbialite-building in the geologic record.

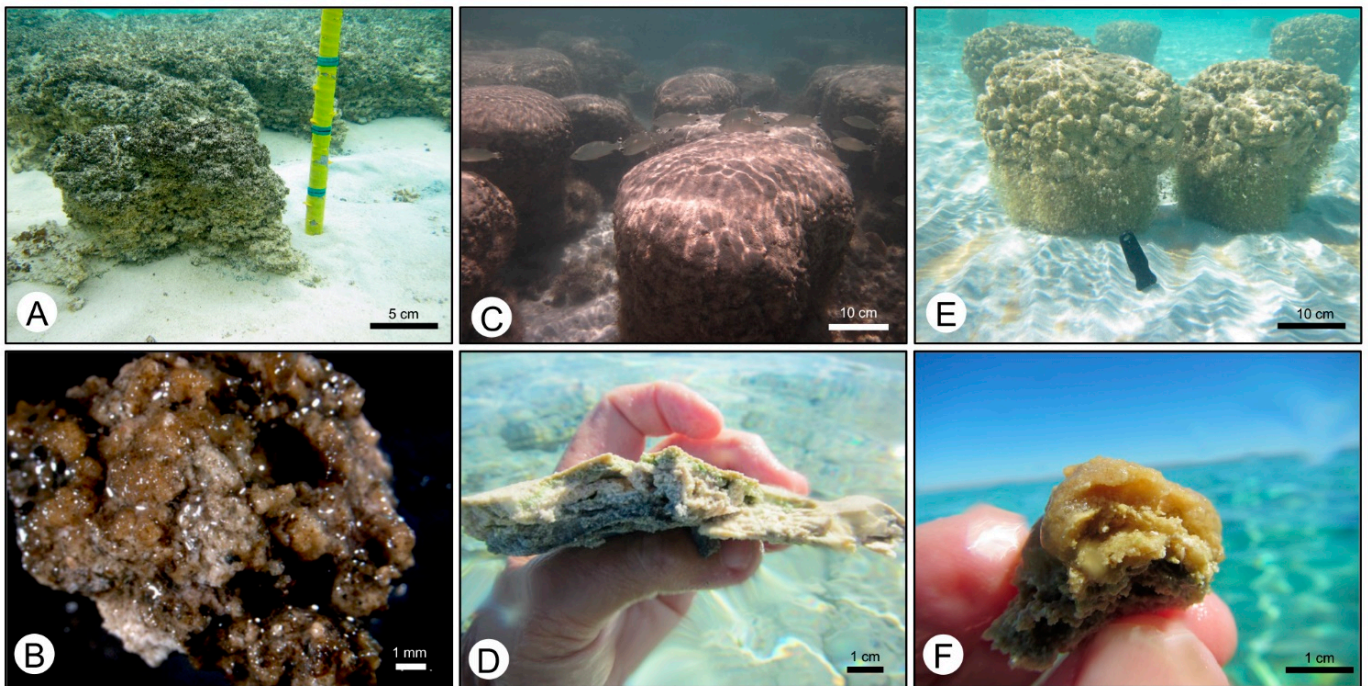


Figure 2. Images showing different morphologies of the three microbialite-forming mat types: pustular mats (A,B), smooth mats (C,D), and colloform mats (E,F).

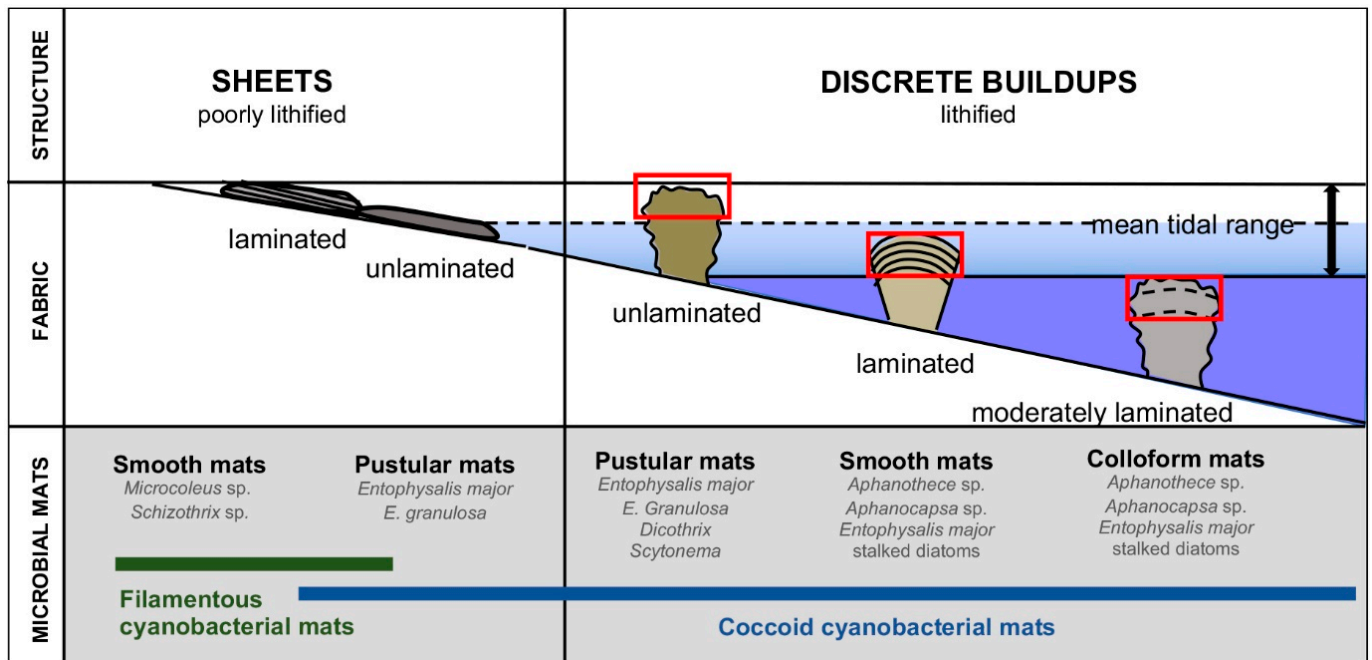


Figure 3. Growth model for microbial structures in Hamelin Pool, modified from Suosaari et al. [11]. Nearshore smooth and pustular mats form poorly lithified sheets; smooth sheet mats are dominated by filamentous cyanobacteria; pustular sheet mats are cocoid. Seaward pustular, smooth, and colloform mats, all enriched in cocoid cyanobacteria, form lithified microbialites. The red boxes highlight degree of lamination in discrete buildups associated with designated mat types.

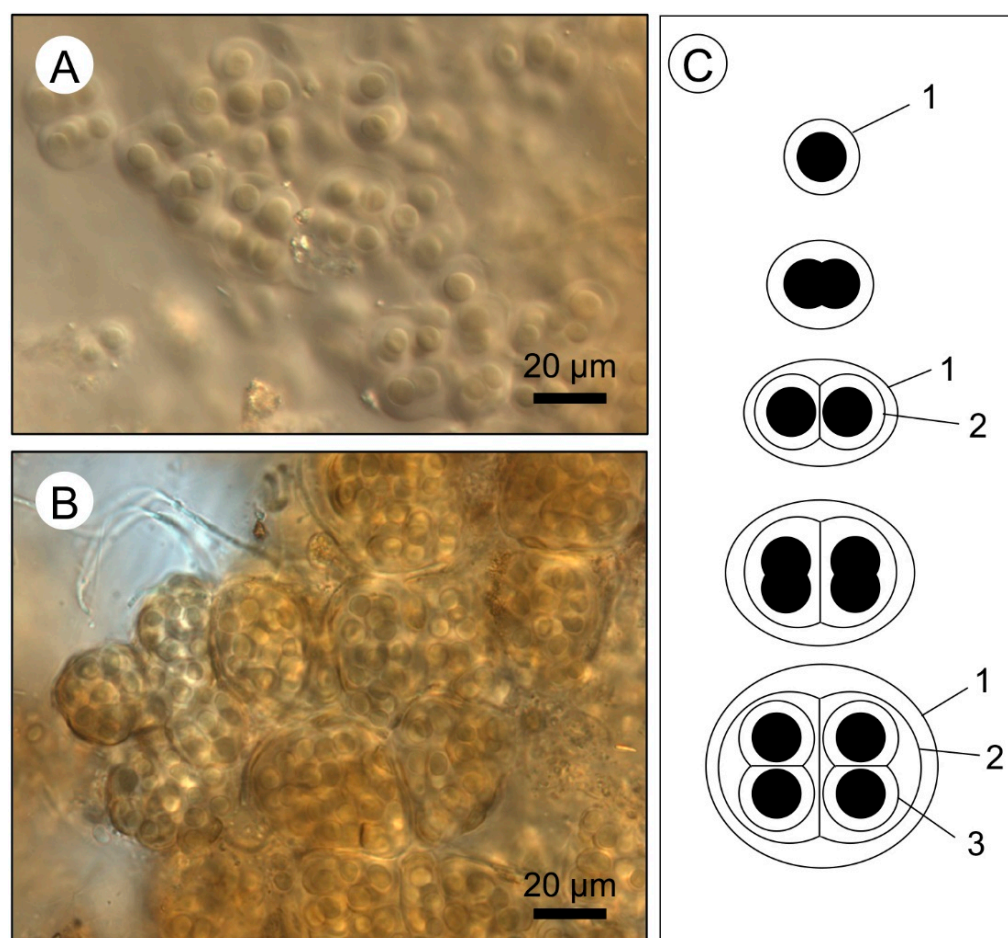


Figure 4. The colonial coccoid *Entophysalis major* (A,B) Light microscopy (DIC) Hamelin Pool samples, HP14_JS12 (A) and HP14_JS03 (B). (C) Drawing showing the division pattern of *Entophysalis*, which generates nested levels of cell envelopes; after Golubic and Hoffman (1976).

3. Materials and Methods

3.1. Terminology

Historically, all microbial buildups in Hamelin Pool have been termed stromatolites, regardless of degree of lamination [23–25,29]. In previous Shark Bay papers e.g., [6,11], we have maintained this historical usage. In the present paper, which focuses on fabric, we differentiate laminated and clotted structures, adopting the terminology of Burne and Moore [1] and Grey and Awramik [4], where microbialites are “organosedimentary deposits that have accreted as a result of a benthic microbial community trapping and binding detrital sediment and/or forming the locus of mineral precipitation”; stromatolites are laminated microbialites, and thrombolites are microbialites with clotted textures.

3.2. Sample Collection

Field work in Hamelin Pool was conducted in March and April 2012, 2013, and 2014. Forty microbial mat samples were collected from microbialite surfaces (Supplemental Table S1). Samples were classified based on the morphology of the mat surface. Seventeen of the field samples were dried and 23 samples were preserved in formalin (Supplemental Table S1).

3.3. Thin Section Preparation

Thirty-four of the 40 microbial mat samples collected from the tops of living microbialite heads (Supplemental Table S1) were made into thin sections. All 17 of the dry samples were embedded in epoxy and sectioned using conventional techniques to a thick-

ness of approximately 30 μm . Additionally, 17 of the 23 preserved samples (Supplemental Table S1) were prepared using ‘wet’ thin section techniques developed by Nye et al. [30], in which samples were kept hydrated throughout the epoxy embedding process in order to preserve the three-dimensional structure of the biological components of the mat and their spatial relationship to the minerals. The resulting wet thin sections, approximately 20 μm thick, were stained with crystal violet, a positively-charged dye that adheres to cell membranes and negatively-charged biomass, thus highlighting the spatial relationship between bacteria cells, EPS, and carbonate.

3.4. Petrographic Analysis

All thin sections were examined using an Olympus BH-2 petrographic microscope with plane-polarized and cross-polarized transmitted light and photographed using a Lumenera Infinity 3 digital microscopy camera (Infinity Analyze v 6.5.6). In order to quantify the abundance of micrite versus grains in the surface mats, 30 thin sections, including 10 pustular mats, 10 smooth mats, and 10 colloform mats (Supplemental Table S2), were scanned at 4800 dpi using a Canon CanoScan 8800F flatbed scanner (MP Navigator EX, Melville, NY, USA). The high-resolution scans were then color coded in Adobe Photoshop CC 2018, with red representing micrite and green representing grains; petrographic observations were used to assist in mapping. The color selection tool and histogram function in Photoshop were used to quantify the number of pixels of each color, giving the relative abundances of micrite versus grains for each mapped thin section.

3.5. Light Microscopy

Light microscopy on sub-samples of the collected mats was done on an Olympus BX-51 fluorescence microscope with a Micropublisher Camera (Q Imaging, Surry, BC, Canada). Confocal scanning laser microscopy (CSLM) was done using a Leica TCS SP 2 (Leica Microsystems, Inc., Mannheim, Germany) as described in [31] excitation was at 488 nm, chlorophyll was detected at 644–722 nm (red), and micrite at 485–492 nm (blue).

3.6. SEM Analysis

Twelve microbial mat samples (Supplemental Table S1) were imaged using the Philips FEI XL-30 Field Emission Scanning Electron Microscope (ESEM/SEM) at the University of Miami Center for Advanced Microscopy. Ten samples preserved in formalin in the field were sequentially dehydrated to 100% alcohol and then fixed using hexamethyldisilazane (HMDS) before being mounted onto stubs and coated with a thin layer of palladium. Images of fractured surfaces of these samples were collected in secondary electron and backscatter electron mode.

Additionally, four billets of microbial mat samples prepared as wet thin sections were examined using SEM (two of these samples are duplicates of fractured surface samples above; Supplemental Table S1). One side of the billet was etched in 2.5% HCl for 10 s, dried, and coated with a thin layer of palladium for imaging using secondary electron mode. The other half of the billet was polished using graduated abrasives up to 0.5 μ grit and imaged using backscatter electron mode.

EDS elemental analysis was used to infer mineralogy. Aragonite and high-Mg calcite mineralogy were differentiated using concentrations of Sr and Mg elements, respectively.

4. Results

4.1. Petrographic Analysis

The grain components, petrographic characteristics of micrite, and visible evidence of microbe–mineral interactions were identified using thin section analysis. While stained wet thin sections were essential for observing microbe–mineral interactions, no significant differences in carbonate components (grains and micrite) were observed between wet and dry sections. Dominant grain types observed in thin sections were quartz and coated quartz,

peloids, and skeletal grains, including the bivalve *Fragum eragatum*, benthic foraminifera, and calcifying green algae—such as *Acetabularia*.

Micrite was common in the surface mats, occurring as dense peloidal micrite and dispersed micrite (Figure 5). Dense peloidal micrite is dark in color; dispersed micrite is lighter, often occurring at the fringes of the dark peloids (Figure 5A,B). In pustular mats, peloidal micrite forms randomly distributed clots (Figure 5A); in smooth and pustular mats, micrite forms along distinct horizons (Figure 5C). At higher magnifications, the micrite often displays a honeycomb texture, reflecting sub-polygonal porosity (Figure 5D).

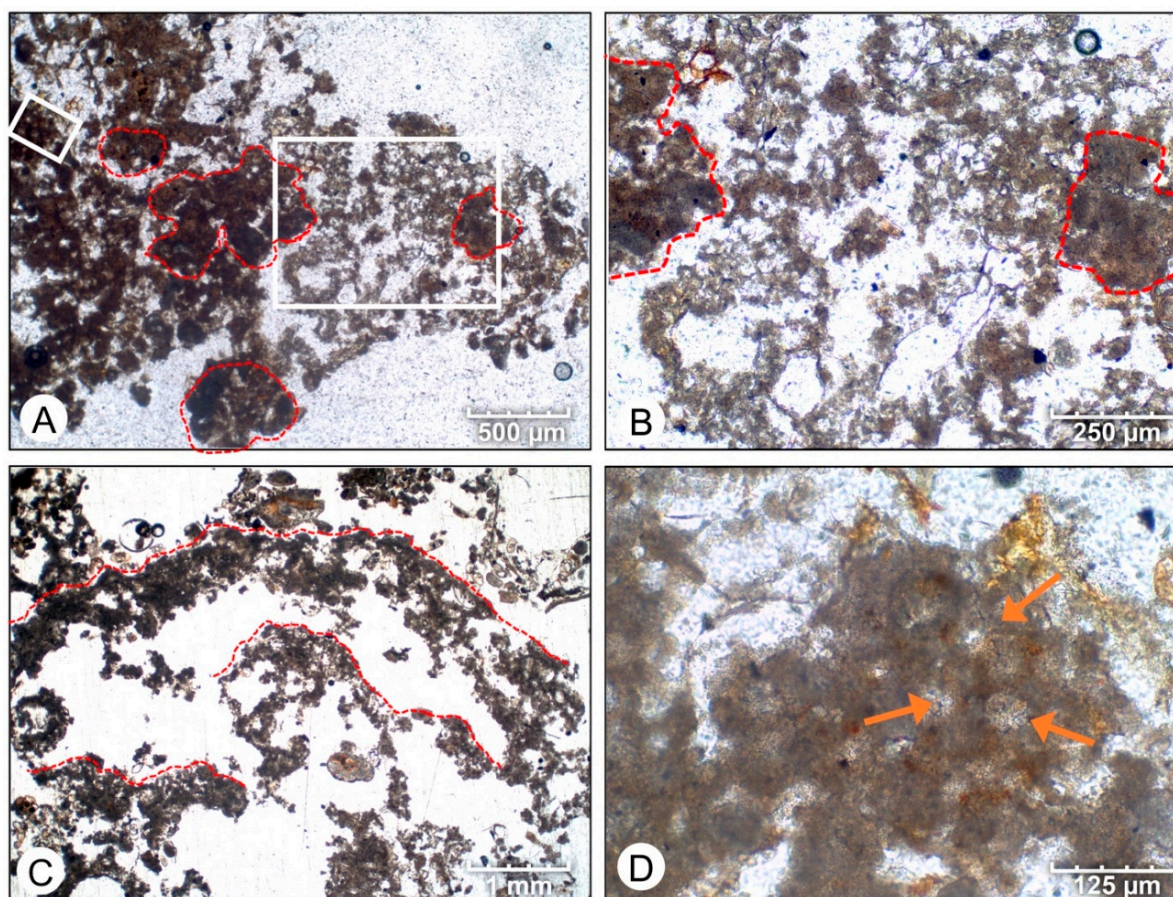


Figure 5. Photomicrographs of micrite in thin sections of dry mat samples. (A) Clots of dark peloidal micrite (outlined in red dashed lines) and dispersed micrite; sample HP13_B36, pustular mat. (B) Higher magnification view of the large box in (A) showing dispersed micrite between clots. (C) Laminae of peloidal micrite (red dashed line); sample HP13_B8, colloform mat. (D) High magnification view of the small box in (A) showing a honeycomb texture in the peloidal micrite due to sub-polygonal porosity (arrows).

Mapping micrite and grains in thin sections scans showed distinct variations in the abundance and distribution of micrite in the different surface mats (Supplemental Figures S4–S6, Supplemental Table S2). The results of this mapping, as summarized in Figure 6, show that pustular mats and colloform mats contained the highest percent of micrite. Pustular mats averaged 81% ($\pm 22\%$, $n = 10$) (Figure 6A, Supplemental Table S3) and micrite is present throughout the mat (Figure 6B). Colloform mats contained an average of 81% ($\pm 16\%$, $n = 10$) micrite (Figure 6A, Supplemental Table S3), with the micrite primarily observed along distinct horizons forming laminae (Figure 6D). Smooth mats contained the least amount of micrite, averaging 36% ($\pm 21\%$, $n = 10$) (Figure 6C, Supplemental Table S3), with the micrite again primarily occurring along distinct horizons forming laminae (Figure 6C).

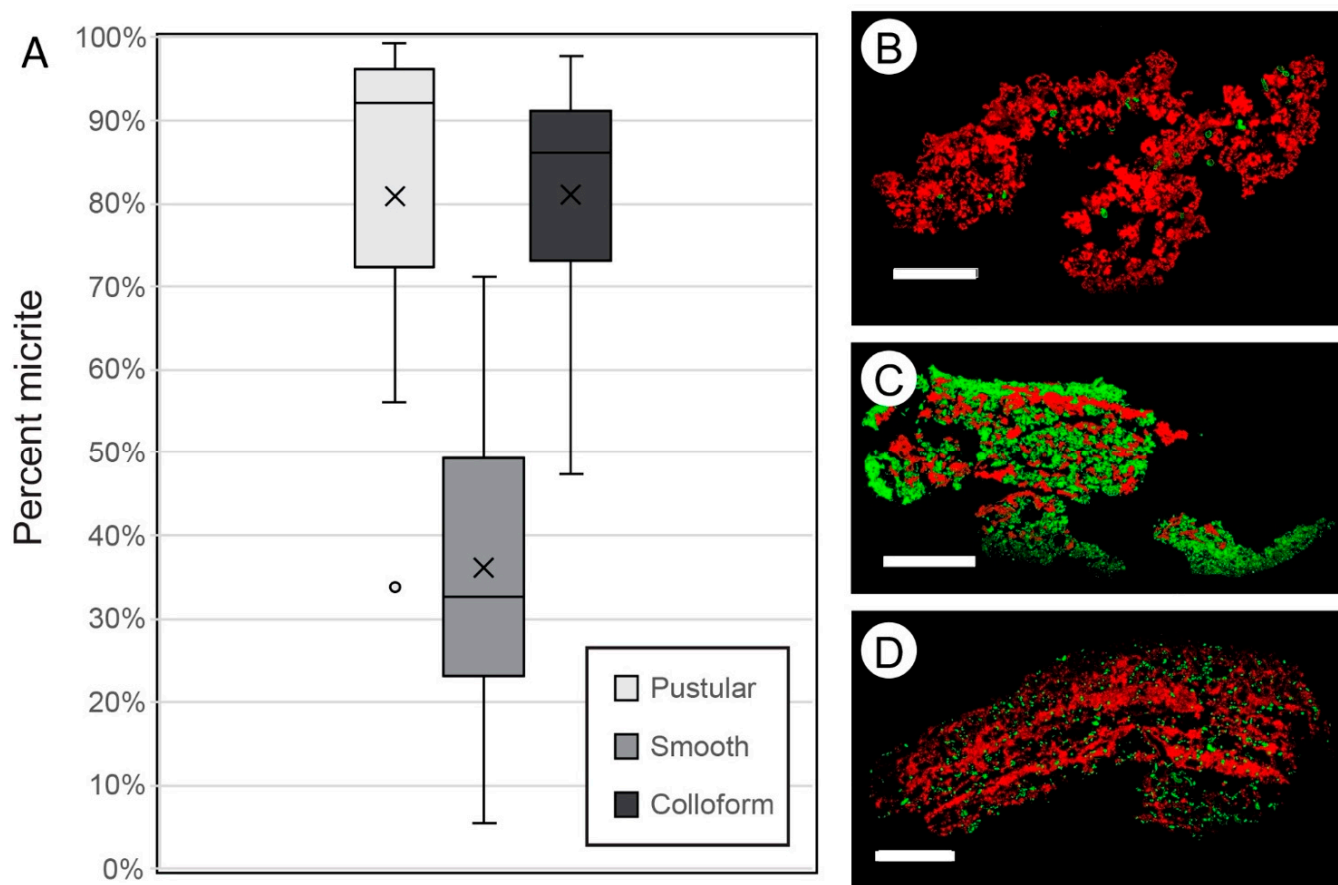


Figure 6. Abundance and distribution of micrite in different mat types. (A) Box and whisker plot showing the mean (x), median (horizontal line), and standard deviation of % micrite in each surface mat type. Pustular mat has an average of 81% micrite, smooth mat has 36% micrite, and colloform mat has 81% micrite. Supporting Data are presented in Supplemental Figures S4–S6 and Supplemental Table S2. (B–D) Examples of mapped thin sections showing micrite (red) vs. grains (green) in a pustular mat with 98% micrite; Sample HP14_JS33 (B), a smooth mat with 36% micrite; sample HP13_B41 (C), and a colloform mat with 72% micrite; sample HP14_JS38c (D). Scale bars in (B–D) are 5 mm.

Crystal violet-stained wet thin sections highlighted organic components in the surface mats, including bacteria, which stained dark purple to blue (color variations reflect different camera settings and changes in color of stain over time), and gelatinous components of the mats, which stained light purple, with scattered dark purple dots representing small coccoid cyanobacteria, such as *Aphanothece* or *Aphanocapsa*. Coccoid cyanobacteria such as *Entophysalis* were abundant in all wet thin sections and were observed as dark purple polka-dots with hollow centers; some colonies exhibited an orange-red tint resulting from the extracellular pigment scytonemine [27].

Wet thin sections revealed intimate spatial relationships between *Entophysalis* cyanobacteria and micrite within all mat types. Pustular mats (Figure 7, Supplemental Figure S1) were commonly composed of large colonies of *Entophysalis*, 100–200 microns in diameter (Figure 7A,B, Supplemental Figure S1A,B) distributed randomly throughout the mat. Micrite precipitation was observed along the edges of these *Entophysalis* colonies, forming networks of large pores, 100–200 μm in diameter (Figure 7B–E) in pustular mats. Additionally, individual *Entophysalis* cells, or small groups of cells, were observed to be enveloped in micrite, forming diffuse micrite and clots with medium and small pores (10–50 μm in size) (Supplemental Figure S1). A confocal image of a pustular mat (Figure 8) shows micrite encapsulating large and small colonies of *Entophysalis* cells.

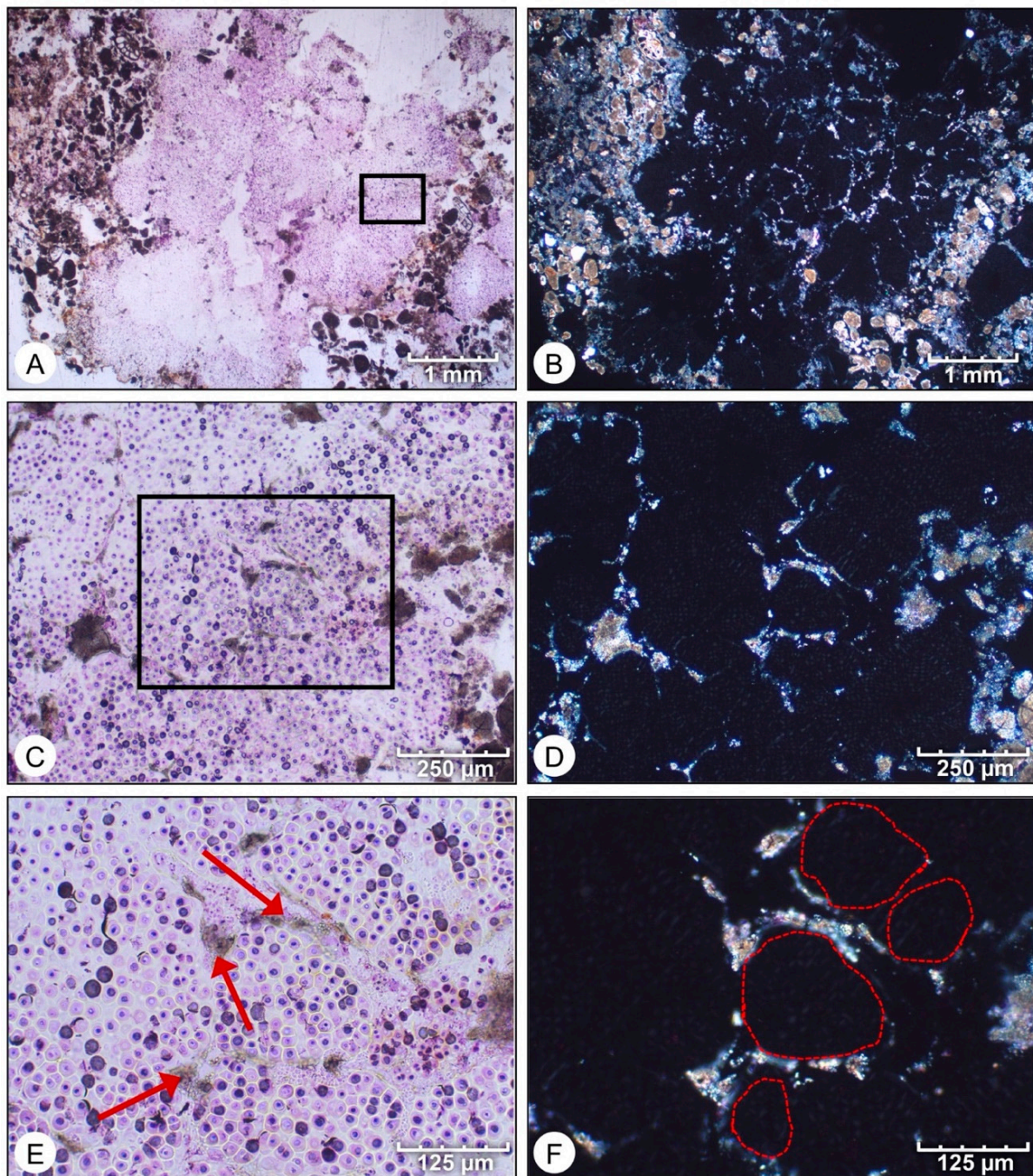


Figure 7. Photomicrographs of wet thin section of pustular mat stained with crystal violet in plane polarized light (A,C,E) and cross-polarized light (B,D,F) at increasing magnifications. Micrite (arrows in E) surrounding large *Entophysalis* colonies (cells are stained dark purple), creating honeycomb structures, ~100 μm in diameter, shown in cross-polarized light (B,D,F, red outlines in F). (C) shows the boxed area in (A), (E) shows the boxed area in (C). Sample HP13_H16carb2.3.

In smooth mats (Figure 9, Supplemental Figure S2), smaller colonies of *Entophysalis*—50 to 100 microns in diameter—are distributed in layers. Micrite is intermixed with the *Entophysalis*, forming weak micritic laminations within a grainy matrix (Figure 9A, Supplemental Figure S2A). Higher magnification images reveal calcification surrounding *Entophysalis* cells and entombment of colonies within the micritic clumps (Figure 9B,C). The images in cross polarized light (Figure 9B,D,F and Supplemental Figure S2B,D,F) show the characteristic features of micrite associated with precipitation surrounding *Entophysalis*: the

micrite commonly has a translucent appearance and is characterized by small (10–20 μm) and medium (20–50 μm) voids, giving the micrite a honeycomb appearance. Voids often contain organic matter when viewed in plane light (Figure 9A,C,E), but appeared as dark voids in cross-polarized light (Figure 9B,D,F). This translucent, honeycomb micrite was easily distinguished from the denser detrital grains, particularly in cross-polarized light (Figure 9D).

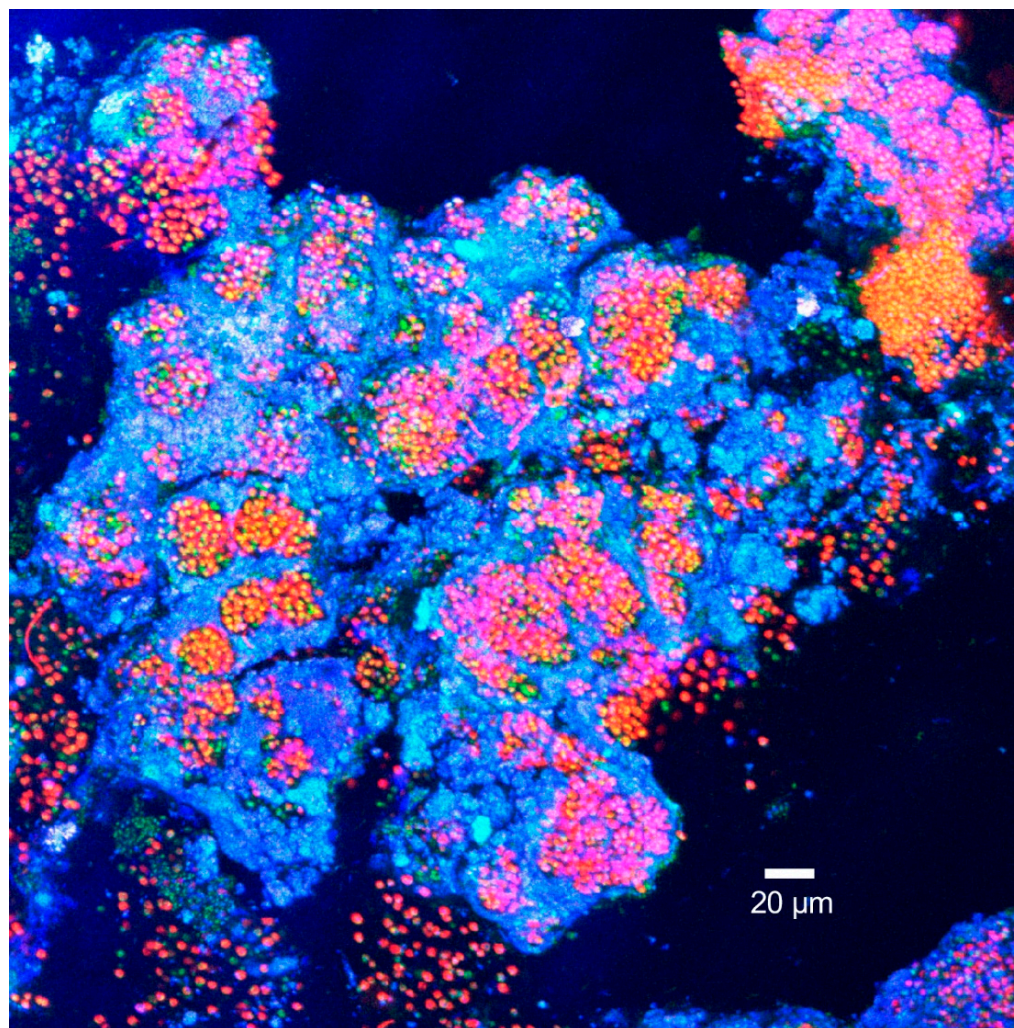


Figure 8. Confocal microscope image showing colonies of *Entophysalis* cells (red to pink or orange dots) surrounded by micrite (blue). Sample HP14-JS21a, pustular mat, formalin fixed.

Wet thin sections of colloform mats (Figure 10; Supplemental Figure S3) also revealed intermixed micrite and *Entophysalis* cells or colonies along distinct micrite-rich horizons (Figure 10A,B; Supplemental Figure S3A,B). Calcification of cell envelopes surrounding individual cells or small clusters of cells formed isolated mini-clots of micrite, which weld together to form larger, irregular clots (Figure 10E) characterized by a network of small- and medium-size pores containing remnant organic matter (Figure 10C–F). The micrite formed in association with *Entophysalis* is distinct in plane-polarized light (Figure 10B,D,F and Supplemental Figure S3B,D,F), with the micrite appearing translucent and containing networks of pore spaces of various sizes—small (~ 20 μm), medium (20–50 μm), and large (100–200 μm) (Figure 10). The resultant pore structures give micrite precipitated in association with *Entophysalis* the characteristic honeycomb texture observed in dry thin sections (Figure 5C).

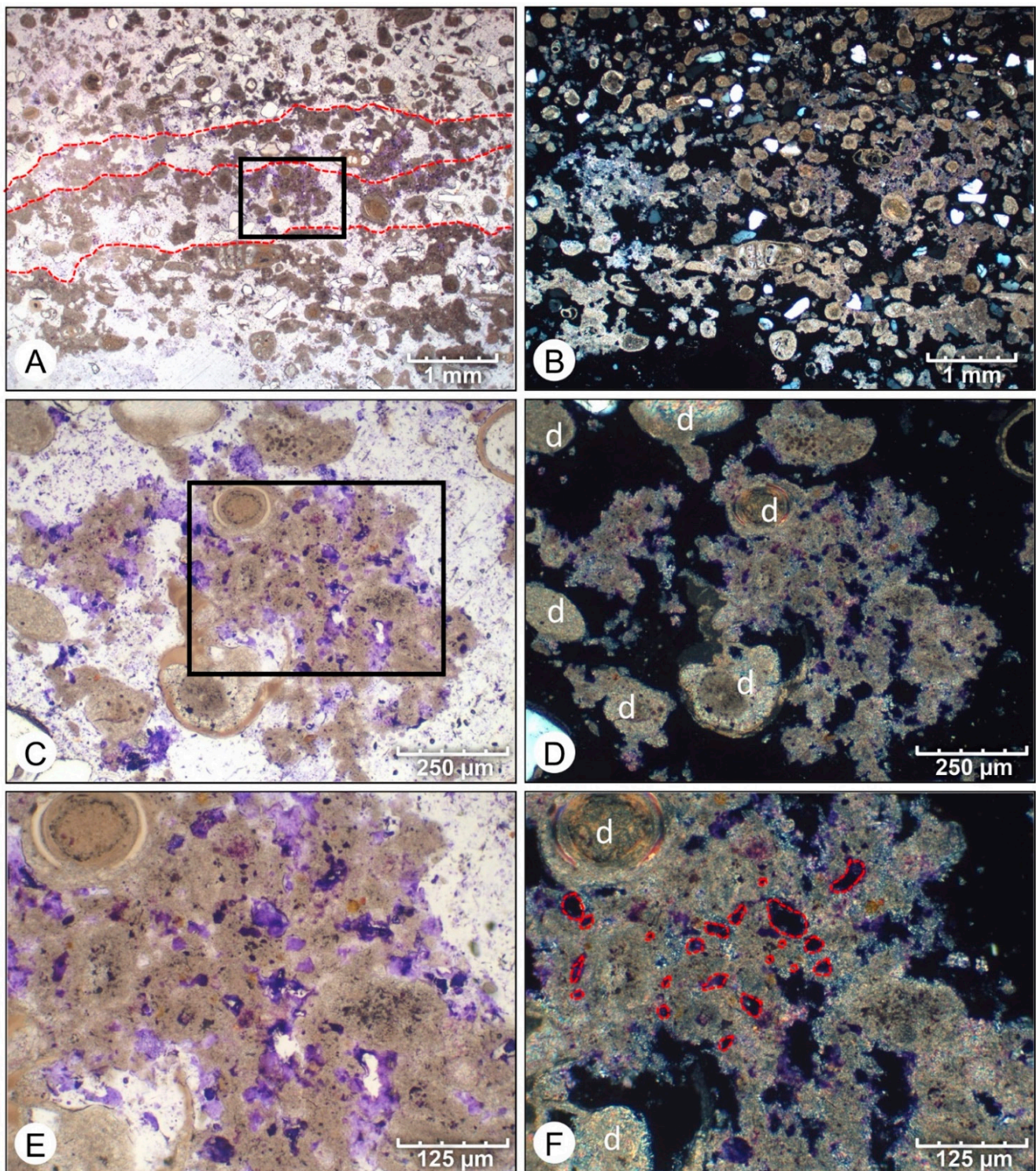


Figure 9. Photomicrographs of wet thin section of smooth mat stained with crystal violet in plane-polarized light (A,C,E) and cross-polarized light (B,D,F) at increasing magnifications. *Entophysalis* and associated micrite are concentrated along sub-horizontal laminae (red dashed lines) in a grain-rich matrix; detrital grains (d in D and F) are distinct from in situ micrite. Calcification of cell envelopes and entombment of *Entophysalis* cells forms micritic clots that appear translucent in cross-polarized light (D,F) and are characterized by small- to medium-sized honeycombs (red dashed lines). (C) shows the boxed area in (A); (E) shows the boxed area in (C). Sample HP14_JS25.

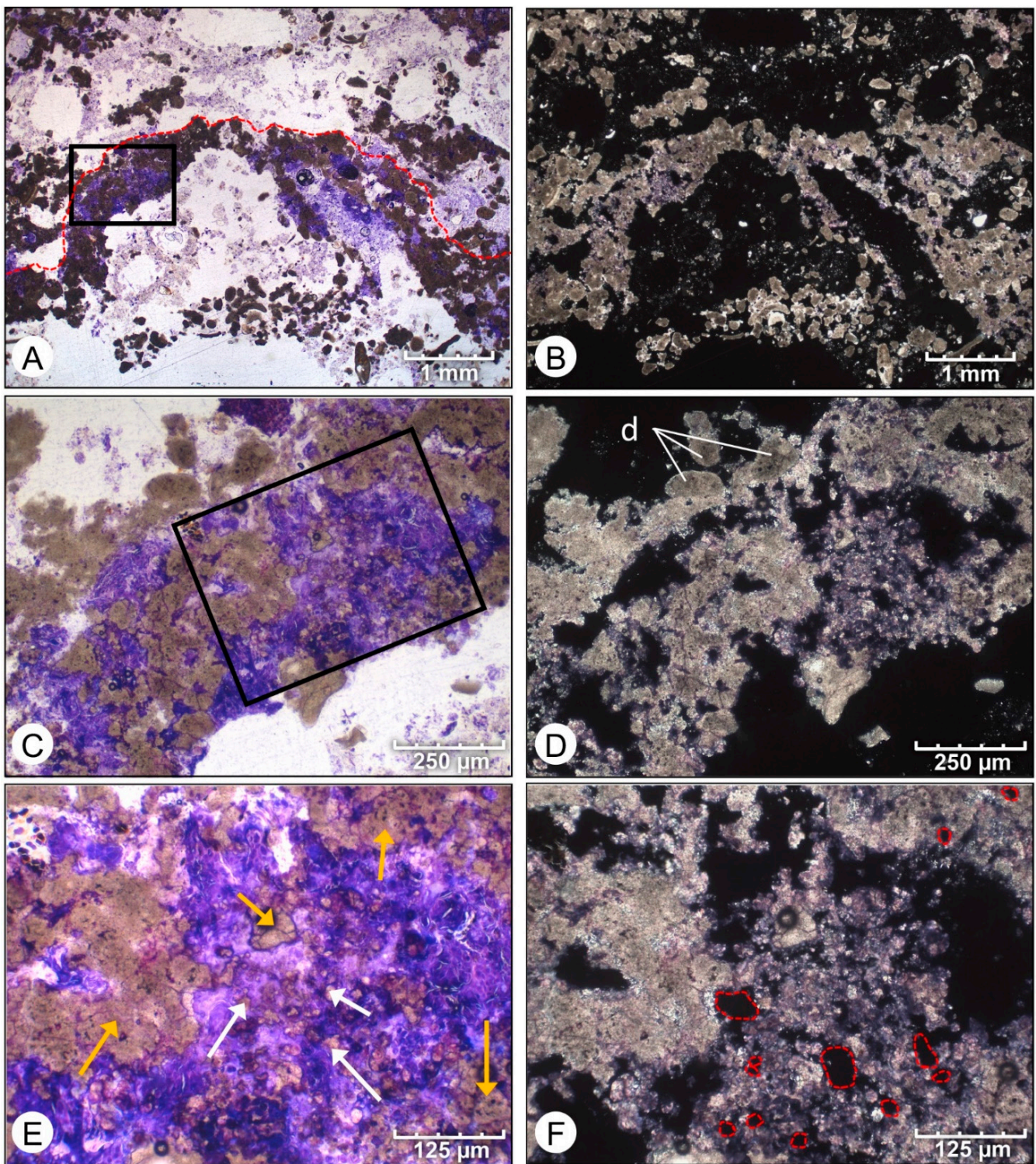


Figure 10. Photomicrographs of wet thin section of colloform mat stained with crystal violet in plane-polarized light (A,C,E) and cross-polarized light (B,D,F) at increasing magnifications. *Entophyalis* and associated micrite are concentrated along convex upward laminae (red dashed line in A). Calcification surrounding *Entophyalis* forms mini-clots of micrite (white arrows, E), which cluster together to form larger clots (orange arrows, E). (C) shows the boxed area in (A); (E) shows the boxed area in (C). (D,F) show the characteristic translucent texture of *Entophyalis* micrite, with small and medium honeycombs (red dashed lines in F). Detrital grains are noted (d in D). Sample HP14_JS38c.

4.2. SEM Analysis

A SEM analysis of fractured, preserved mat samples revealed an abundance of coccoid colonies, presumed to be *Entophysalis* (Figure 11). These *Entophysalis* colonies were often embedded within EPS (Figure 11A,B). Cross-sections through fractured samples displayed the classic honeycomb textures (Figure 11B), with *Entophysalis* colonies embedded within EPS and empty pockets that previously contained coccoid cells. Tiny crystals, ranging in size from 100 nm to microns in diameter, were also observed within the EPS coatings (Figure 11C–F). Crystal shape ranged from sub-micron anhedral nano-bulbous spheres (~100 nm) (Figure 11D,F) to micron-sized tabular and rod-shaped crystals (Figure 11F). EDS spectra indicating the presence of Ca and O, minor Sr, and lack of Mg, suggest aragonite mineralogy.

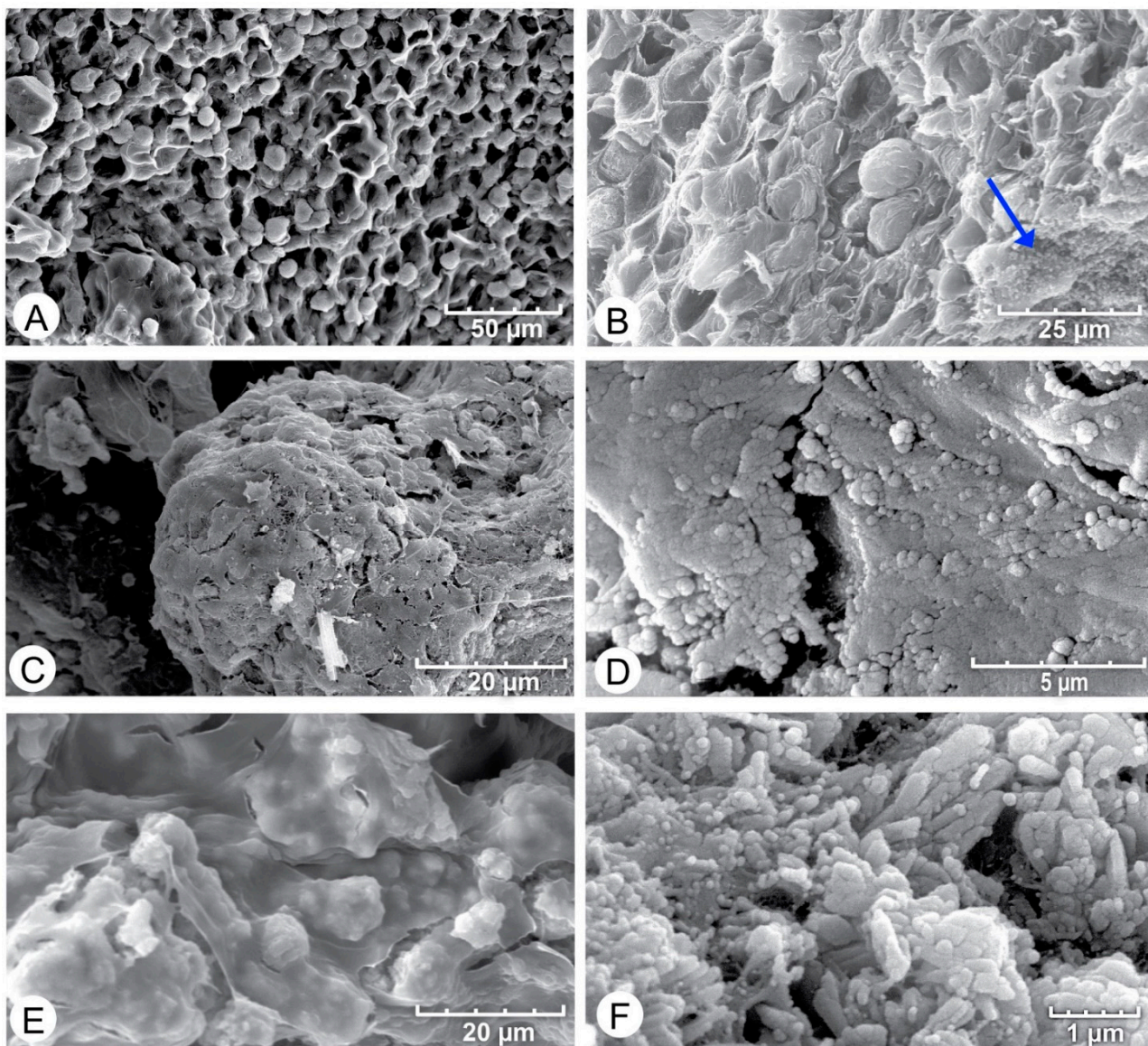


Figure 11. SEM images of calcifying *Entophysalis* in fractured sections of preserved samples. (A) Coccoid cells in a honeycomb EPS matrix; Sample HP13_H16carb2.3, pustular mat. (B) Crystals (blue arrow) forming in the honeycomb EPS matrix. Sample HP14_M96a, pustular mat. (C) EPS with embedded crystals coating *Entophysalis* colonies; sample HP14_M96a, pustular mat. (D) Magnified view of sample HP14_M96a showing nanobulbous carbonate on EPS surface. (E) Crystal aggregates embedded within EPS; sample HP12_19.1, colloform mat. (F) Gradation from nanobulbous (left) to tabular and rod-shaped crystals (right) in sample HP14_JS03, pustular mat.

Etched wet thin sections observed with SEM showed that areas of dense peloidal micrite (Figure 12) again show micron to sub-micron sized nanobulbous to tabular and rod-shaped crystals (Figure 12B,C). Purple-stained holes within the micrite, as seen in wet thin sections, appear as pits in SEM (Figure 12A,C), producing an overall honeycomb structure.

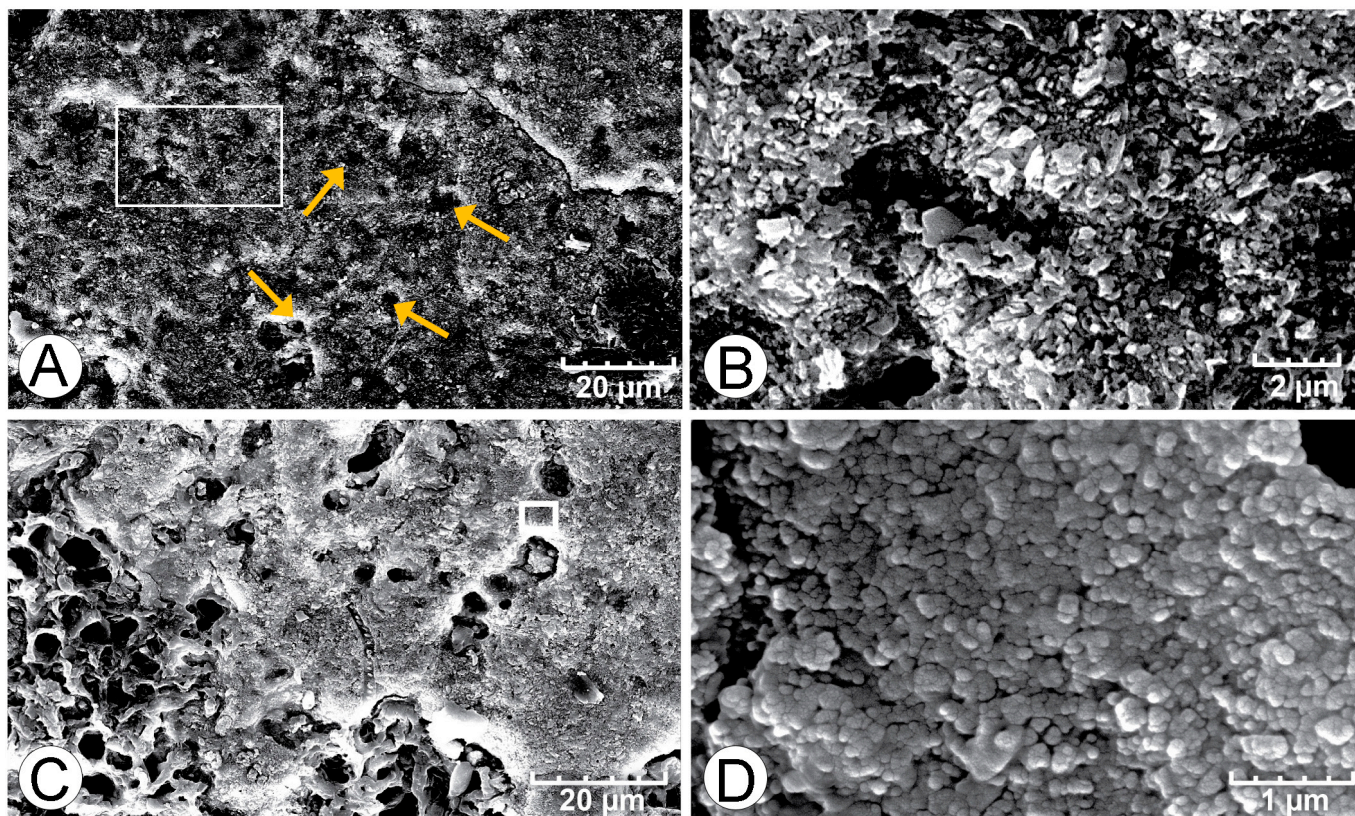


Figure 12. SEM photomicrographs showing micrite in etched wet thin sections of pustular mats. (A,B) Sample HP14_JS03 showing dense micrite with distinct pits, about ~5 micron in size (yellow arrows), forming a honey comb texture. High magnification view in (B) shows details of the white box in (A), with rod-shaped to tabular crystal morphology. (B,C) Sample HP13_H16carb, showing dense micrite with ~5 micron voids forming honeycomb textures. High magnification view in (D) shows details of the white box in (C), with nanobulbous crystal morphology.

5. Discussion

The results above provide a basis for evaluating micrite precipitation as a primary accretion mechanism in Hamelin Pool microbialites, identifying the origin of the micrite, and discussing the effect of microbes on micritic textures. These topics revise microbialite growth models in Hamelin Pool and underscore the role of these structures as analogs of ancient microbialites.

5.1. What Are the Amounts and Distribution of Micrite?

New estimates of in situ micrite precipitation in microbial mats on the surfaces of Hamelin stromatolites, as documented in this study, indicate the importance of micrite precipitation as a primary accretion mechanism in this iconic locale. As reported above, micrite precipitation accounts for an average of 81% of initial accretion by pustular mats, 36% of initial accretion by smooth mats, and 81% of accretion by colloform mats forming discrete structures. In pustular mats, precipitated micrite forms clots that are distributed randomly throughout the mat; micrite forming in smooth and colloform mats is concentrated along distinct horizons, forming laminae.

5.2. What Is the Origin of Micrite?

Several lines of evidence indicate that the micrite observed within the surface mats is not fine-grained detrital grains that are trapped and bound, but instead is precipitated in situ in close association with microbes. The dense, uniform texture of the micrite and lack of skeletal debris observed in SEM (Figures 11 and 12) are characteristic of in situ precipitates, contrasting with transported mud, which is typically a mixture of clay and silt [32,33]. In particular, the nanobulbous texture of micrite in all mat types in Hamelin Pool (Figure 11D) is typical of calcium carbonate produced in association with microbial EPS [9,34]. Initial precipitation in a microbial mat often starts as an amorphous gel within an EPS matrix, followed by the production of nanospheres, which act as seeds for further carbonate crystallization [9,35–37]. The nanobulbous to tabular and rod-shaped crystals in the clotted peloidal micrite associated with coccoid cells (Figures 11 and 12) provides strong evidence for the role of bacteria in micrite precipitation in all three mat types.

5.3. Do Microbes Influence the Micritic Textures?

As shown in Figures 7–10, *Entophysalis* and micrite are closely associated in pustular, smooth, and colloform mats throughout Hamelin Pool. In particular, mineralization appears to occur around cell envelopes of *Entophysalis* cells, producing honeycomb structures. Similar “web-like” or “nanoporous” structures have been used in fossil carbonate structures as indicators of biogenicity, particularly as evidence of coccoid cyanobacteria, where fossilized cells are lacking [38,39].

Our observations further suggest that the dominant pathway to micrite precipitation in the surface mats of Hamelin Pool microbialites is the calcification of the cell envelopes surrounding *Entophysalis* cells and/or colonies. Wet thin sections show the precipitation of micrite associated with *Entophysalis* cell envelopes, (Figures 7–10, Supplemental Figures S1–S3). In pustular mats, the micrite forms clots associated with large clusters of *Entophysalis* cells (Figure 7, Supplemental Figure S1); in smooth and colloform mats, smaller colonies of *Entophysalis* are concentrated in layers, and micrite forms laminae (Figures 9 and 10, Supplemental Figures S2 and S3). Comparative metagenomic and functional gene analyses by Babilonia et al. [26] showed the enrichment of photosynthetic pathways in pustular mats, and the heterotrophic metabolism in smooth and colloform mats. These data suggest that micrite in pustular mats may result from alkalinity production by cyanobacteria and anoxygenic phototrophs, while micrite formation in smooth and colloform mats may be associated with heterotrophic communities e.g., [9,40–42]. Additional geochemical analyses, such as stable isotope (i.e., C, N, O, S) and elemental compositions of the micrite, will likely refine precipitation mechanisms.

A schematic drawing in Figure 13 shows hypothetical scenarios for forming different scales of honeycomb texture by the calcification of cell envelopes surrounding *Entophysalis* colonies. With every generation of cell division, a new cell envelope is formed, with the oldest sheaths located towards the exterior and the youngest sheaths forming closest to the individual cells (Figure 4). Each row of Figure 13 depicts possible patterns of calcification based on colony age, resulting in micritic textures ranging from ‘small’ (10–20 μm) to ‘large’ (100–200 μm) honeycombs. Row A is composed of ‘young’/immature *Entophysalis* that has undergone limited cell division and therefore has fewer generations of cell envelopes (Figure 13). Initial calcification occurs along the outermost layer of this young *Entophysalis* cell and/or colony, which results in small honeycombs. Rows B and C are composed of mature *Entophysalis*, which has undergone multiple generations of cell division. The difference between Rows B and C is that calcification can occur either within the colony, along the innermost and youngest cell envelopes (Row B), resulting in small to medium honeycombs as observed in smooth and colloform mat types (Figures 10 and 11), or along the outer, oldest cell envelopes (Row C), resulting in large honeycombs as observed in the pustular mat type (Figure 9). Note that Rows A and B both produce similar micritic textures with ‘small’ honeycombs; these small structures could be formed either through early calcification of the cell envelopes of immature coccoids (Row A) or late calcification of

the cell envelopes of mature coccoids (Row B). As such, the conceptual model of Figure 13 has implications for considering the dominant metabolisms that could lead to micrite precipitation in the different mat types.

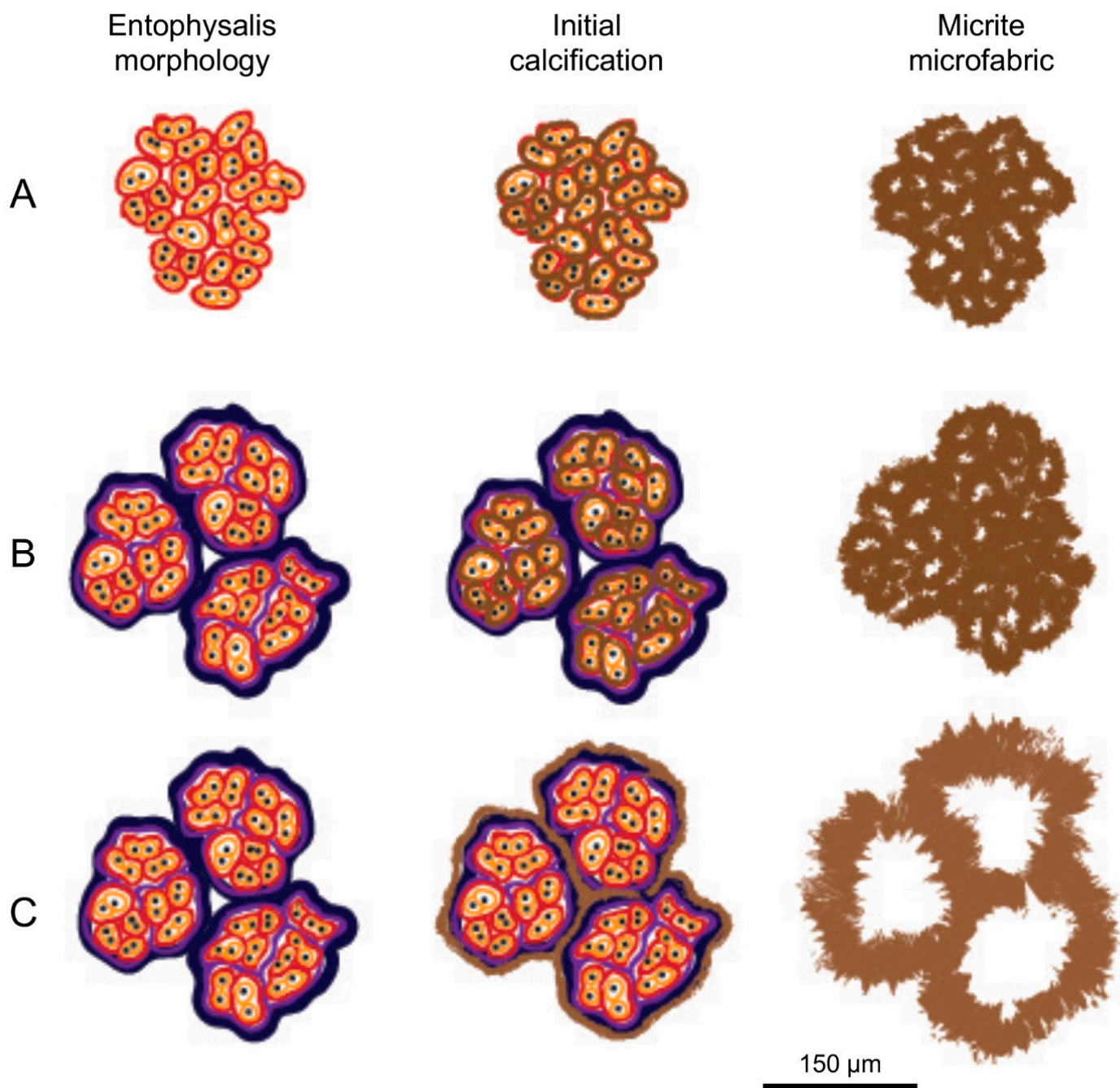


Figure 13. Cartoon illustrating different levels of calcification of *Entophysalis*, resulting in distinct micritic microfabrics. Individual *Entophysalis* cells are shown as black dots. Different generations of encapsulating cell envelopes are shown in different colors, with navy being the oldest cell envelope and yellow being the youngest. See text for explanation of the different scenarios shown in rows (A–C).

According to the conceptual model presented in Figure 13, the sizes of the honeycomb structures may provide insight into the maturity of the *Entophysalis* colony when calcification occurs. For example, smaller holes within dense peloidal micrite in smooth and colloform mats (Figures 9 and 10, Supplemental Figures S2 and S3) may result from

the calcification of younger *Entophysalis* colonies, which have not undergone many cell divisions, whereas larger honeycomb structures observed in peloidal micrite forming in pustular mats (Figure 8, Supplemental Figure S1) may reflect the calcification of older *Entophysalis* colonies with multiple generations of cell divisions. Moreover, pustular mats are periodically subaerially exposed [11,23,24,43,44], which may lead to the preferential degradation of the older, outermost sheath and/or evaporitic precipitation of carbonate during exposure [9,45], thereby leading to large honeycomb textures.

6. Implications

The recognition of *Entophysalis* as a major source of microbial micrite in initial accretion by pustular, smooth, and colloform mats on the surfaces of Hamelin Pool stromatolites has significant implications for understanding accretion by living microbialite-forming microbial mats in Shark Bay and may provide insight into the interpretation of ancient structures.

6.1. Mat Community and Initial Accretion

Recognition that all three stromatolite-forming mats in Hamelin Pool are dominated by coccoid cyanobacteria, in particular *Entophysalis*, contrasts with earlier reports describing microbial communities of surface mats. All previous studies have recognized *Entophysalis* as the dominant component of pustular mats e.g., [17,24,25,44,46,47], with calcification of coccoid sheaths resulting in micrite precipitation. However, Logan et al. [24], Playford [25] and Playford et al. [23] described smooth mats as filamentous, composed mainly of *Schizothrix*, and colloform mats as dominated by the filamentous cyanobacteria *Microcoleus* and *Schizothrix*, as well as diatoms. Golubic [47] and Jahnert and Collins [17,44,48] recognized that colloform mat communities contained coccoid cyanobacteria, but again described smooth mats as filamentous. These previous studies describing smooth mats as filamentous may have sampled nearshore smooth sheet mats, which are filamentous and do not build structures with significant relief [11] (Figure 3), rather than smooth structure-forming mats on intertidal to subtidal microbialites surfaces, which are dominated by coccoid cyanobacteria (Figure 3).

Furthermore, our observations shift the focus of stromatolite growth in an iconic modern setting from agglutination of coarse-grained sediment, as commonly emphasized by previous authors e.g., [14,15,49], to precipitation of micrite. Our results show that the calcification of the cell envelopes of *Entophysalis* in all three mat types form micrite, which accounts for averages between ~30% to ~80% of initial microbialite accretion (Figure 4). These results extend observations by Reid et al. [6], who recognized the importance of in situ micrite precipitation as a primary accretionary mechanism of Hamelin Pool microbialites, but did not identify the source of the micrite, now recognized as microbial in origin. Jahnert and Collins [44] also recognized micrite as a common component of the Hamelin Pool microbialites, ascribing primary accretion to trapping and binding with subsequent micrite formation during lithification and grain micritization [44].

Still lacking in our understanding of initial accretion in Hamelin Pool microbialites is the cause of lamination in smooth and colloform mats. Thin section observations (Figures 9 and 10) show that lamination results from episodic concentrations of *Entophysalis* and associated micrite precipitation arranged in horizons. Golubic [46] suggested that carbonate precipitation associated with *Entophysalis* in unlaminated mamillated (pustular) mats occurred mostly in austral summer, leading to hard surfaces that are colonized by endoliths. While some pustular mats in the upper intertidal zone become hard and knobby with the development of a film mat, most pustular, smooth, and colloform mats containing calcified *Entophysalis* are lightly lithified and lack endolith colonization, and we have not observed that calcification of *Entophysalis* is seasonal (unpublished field observations). Determining factors responsible for the episodic concentration of *Entophysalis* in horizons in smooth and colloform mats, leading to micrite precipitation and lamination, warrants future research. It is important to note that the fabrics described in this paper

are those formed by surface mats in the upper centimeter or two of the heads. Moreover, these initial fabrics serve as a template for a downward evolution of fabrics within the microbialite structures.

6.2. Significance to the Geologic Record and Beyond

Recognition that coccoid-dominated microbial communities form laminated fabrics in smooth and colloform mats in Hamelin Pool (see Supplemental Figures S5 and S6) is relevant for the interpretation of fossil structures in the geologic record. Since direct cellular preservation in carbonate rocks is typically rare [38,50–53], sedimentary structures are sometimes used as proxies of the microbial communities interpreted to form them. Lamination in fossil microbialites has traditionally been linked to filamentous microbes, with unlaminated clotted textures attributed to coccoid-dominated communities [54,55] and references therein. This concept is reinforced by more recent studies that explicitly or implicitly link lamination to filamentous microbes e.g., [56,57]. Our observations showing laminae formed by living, coccoid-dominated microbial communities are evidence for the potential role of coccoids in lamination formation.

In addition, our dataset provides a modern analog for fossil microbialites formed through a combination of trapping and binding and micrite precipitation. In a comprehensive review, Suarez-Gonzalez et al. ([57]: Table 2) identified twelve localities, ranging in age from Late Devonian to Late Pliocene, with structures composed of varying proportions of sediment and micrite. In analyzing these fossil examples, Suarez-Gonzalez et al. [57] proposed that sediment accretion by trapping and binding was controlled by specific environmental factors. Hamelin Pool would be an ideal environment to test these hypotheses.

Finally, it is of interest to note that the dominant microbe associated with micrite precipitation in Hamelin microbialites, *Entophysalis*, has an ancient lineage linked to *Eoentophysalis* sp., a coccoid that was common throughout early and middle Proterozoic stromatolite assemblages [27]. Impressively, this is one of the longest biological lineages known in the geological record [46]. Detailed investigations of processes of calcification of *Entophysalis* in Hamelin Pool may provide insight into precipitation mechanisms in these ancient ecosystems. Finally, micrite precipitation associated with *Entophysalis* in Hamelin Pool mats produces structures and microscale fabrics that may indicate the presence of life based on carbonate microtexture alone, despite a lack of preserved microfossils. In particular, the honeycomb structures produced by the calcification of the cell envelopes and entombment of *Entophysalis* shown in this paper are likely a characteristic biosignature. Similar textures thought to be associated with microbial communities and EPS calcification have been observed throughout time and space. Examples include microfossil assemblages from the Precambrian Strelley Pool Formation in the Pilbara Craton, Western Australia [58] thrombolites from the Cambrian Zhangxia formation, Shandong Province, China [59] bituminous limestones from the Late Devonian (Figure 14) [38] microbial carbonates from the Lower Cretaceous Codó Formation (north-east Brazil) [60] laminites of the Cretaceous Crato Formation in the Araripe Basin, northeastern Brazil [61] lithified stromatolite mats of Pleistocene age from the Gulf of California, Mexico [62] etc., along with many other locations in the modern i.e., [63–68] etc. In addition, entombed organic matter within micritic horizons, as observed here in both smooth and colloform mats (Figures 7–10), are targets for extractable biomarkers [51,53] in ancient carbonate environments on Earth and elsewhere in the universe *sensu* [53].

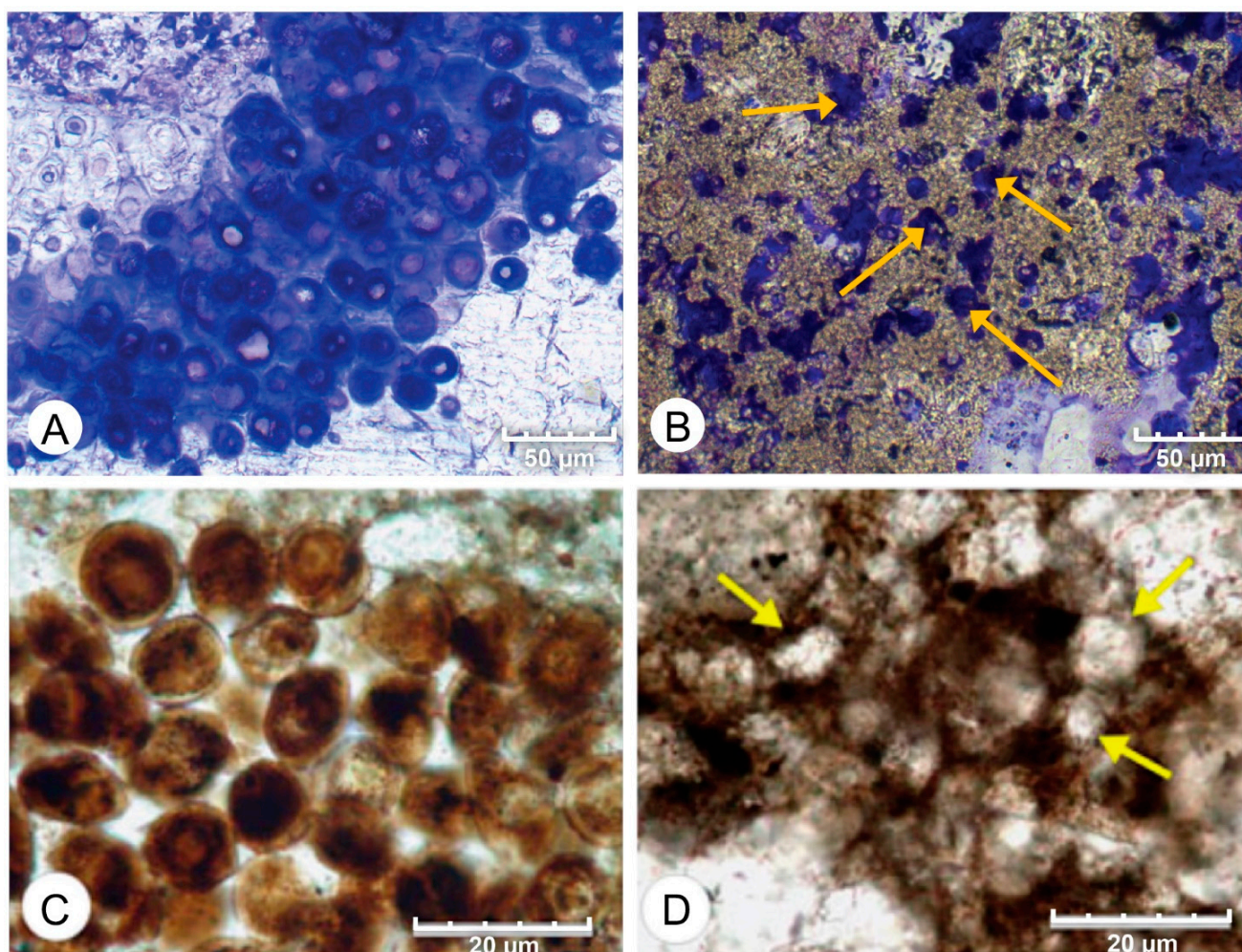


Figure 14. Comparison of petrographic characteristics of modern and ancient coccoid cyanobacteria. (A,B) Photomicrographs of wet, thin section HP14_JS38b from Hamelin Pool stained with crystal violet. (A) shows distinct cells of *Entophysalis*. (B) shows inclusions of *Entophysalis* within micrite (arrows). (C) Photomicrographs of groups of coccoid cyanobacteria from the Late Devonian preserved in bituminous limestone of the Lagow profile. (D) Strongly-degraded fragments of the same mat as (C) where the remains of the coccoid cells have been mineralized with fine-grained calcium carbonate (arrows). The mineralized coccoid remains exhibit a honeycomb pattern similar to that formed by entrapped coccoid cells in the image above (B). (C,D) from [38]. Reproduced with permission from Geobiology; published by John Wiley and Sons, 2012.

7. Conclusions

Key findings of the present study are summarized below.

1. In situ precipitation of micrite is an important accretion mechanism in Hamelin Pool microbialites, averaging 36% to 81% of accretion in surface mats.
2. Wet thin sections of surface mats from microbialites reveal intimate relationships between *Entophysalis* cyanobacteria and micrite across all mat types (pustular, smooth, and colloform). This is of particular interest as *Entophysalis* is a living analog of *Eoentophysalis*, a coccoid cyanobacteria commonly found throughout early and middle Proterozoic stromatolite assemblages.
3. Initial micrite distribution within each mat type reflects the size and distribution of *Entophysalis* colonies within the surface mats. Random clots of micrite within pustular mats reflect the occurrence of large colonies of *Entophysalis* distributed randomly

throughout the mat. Micrite in smooth and colloform mats is aligned along horizons that are enriched in smaller *Entophysalis* colonies and forms laminae.

4. Micrite formed by the calcification of *Entophysalis* cell envelopes in Hamelin microbialites has a characteristic honeycomb appearance resulting from the entombment of cells or colonies, with the size of honeycombs hypothesized to reflect the maturity of the *Entophysalis* community. Crystal shapes range from nanobulbous to tabular or rod-shaped, with an aragonite mineralogy.
5. Our observations redefine our understanding of microbialites accretion in Hamelin Pool stromatolites, showing that primary microbial micrite is important in the accretion of these living structures and that coccoid mats are capable of producing laminated structures.

Supplementary Materials: The following supporting information can be downloaded at: <https://www.mdpi.com/article/10.3390/geosciences12080304/s1>, Figure S1: Wet thin sections of pustular mat, Figure S2: Wet thin sections of smooth mat, Figure S3: Wet thin sections of colloform mat, Figure S4: Mapped pustular mat thin sections showing micrite vs. grains, Figure S5: Mapped smooth mat thin sections showing micrite vs. grains, Figure S6: Mapped colloform mat thin sections showing micrite vs. grains, Table S1: Metadata for field samples, Table S2: Mapped thin sections for percent micrite, Table S3: percent micrite statistics for each mat type.

Author Contributions: B.E.V., E.P.S. and R.P.R. wrote the main manuscript text. B.E.V., E.P.S., J.F.S., A.M.O. and R.P.R. conducted field work. B.E.V., J.F.S. and R.P.R. conducted laboratory analysis. All authors reviewed and edited the manuscript. All authors have read and agreed to the published version of the manuscript.

Funding: This project was funded by Chevron, BP, Repsol, and Shell.

Acknowledgments: We thank Phil Playford for inspiration and guidance; the Geological Survey of Western Australia and Hamelin Station for logistical support; the Western Australian Department of Parks and Wildlife (formerly Department of Environment and Conservation); and the federal Department of Sustainability, Environment and Population and Communities for field access and sampling permits. The manuscript benefited from comments by Pablo Suarez-Gonzalez and an anonymous reviewer. Hamelin Stromatolite Contribution #9.

Conflicts of Interest: The authors declare that they have no known competing financial interests or personal relationships that could have appeared to influence the work reported in this paper.

References

1. Burne, R.V.; Moore, L.S. Microbialites: Organosedimentary Deposits of Benthic Microbial Communities. *Palaios* **1987**, *2*, 241–254. [[CrossRef](#)]
2. Awramik, S.M.; Grey, K. *Stromatolites: Biogenicity, Biosignatures, and Bioconfusion*; SPIE: Bellingham, WA, USA, 2005; Volume 5906, 59060p. [[CrossRef](#)]
3. Walter, M.R. Stromatolites: The Main Geological Source of Information on the Evolution of the Early Benthos. In *Early Life on Earth*; Nobel Symposium No. 84; Bengtson, S., Ed.; Columbia University Press: New York, NY, USA, 1994; pp. 270–286.
4. Grey, K.; Awramik, S.M. *Handbook for the Study and Description of Microbialites*; Geological Survey of Western Australia: Perth, Australia, 2020; ISBN 9781741688610.
5. Riding, R. Microbial Carbonates: The Geological Record of Calcified Bacterial-Algal Mats and Biofilms. *Sedimentology* **2000**, *47*, 179–214. [[CrossRef](#)]
6. Reid, R.P.; James, N.P.; Macintyre, I.G.; Dupraz, C.P.; Burne, R.V. Shark Bay Stromatolites: Microfabrics and Reinterpretation of Origins. *Facies* **2003**, *49*, 299–324. [[CrossRef](#)]
7. Thompson, J.B.; Ferris, F.G. Cyanobacterial Precipitation of Gypsum, Calcite, and Magnesite from Natural Alkaline Lake Water. *Geology* **1990**, *18*, 995–998. [[CrossRef](#)]
8. Stolz, J.F.; Feinstein, T.N.; Salsi, J.; Visscher, P.T.; Reid, R.P. TEM Analysis of Microbial Mediated Sedimentation and Lithification in Modern Stromatolites. *Am. Mineral.* **2001**, *86*, 826–833. [[CrossRef](#)]
9. Dupraz, C.; Reid, R.P.; Braissant, O.; Decho, A.W.; Norman, R.S.; Visscher, P.T. Processes of Carbonate Precipitation in Modern Microbial Mats. *Earth-Science Rev.* **2009**, *96*, 141–162. [[CrossRef](#)]
10. Mann, S. *Biomineralization: Principles and Concepts in Bioinorganic Materials Chemistry*; Oxford chemistry masters; Oxford University Press: Oxford, UK, 2001; ISBN 9780198508823.
11. Suosaari, E.P.; Reid, R.P.; Playford, P.E.; Foster, J.S.; Stolz, J.F.; Casaburi, G.; Hagan, P.D.; Chirayath, V.; Macintyre, I.G.; Planavsky, N.J.; et al. New Multi-Scale Perspectives on the Stromatolites of Shark Bay, Western Australia. *Sci. Rep.* **2016**, *6*, 20557. [[CrossRef](#)]

12. Suosaari, E.P.; Pamela Reid, R.; Oehlert, A.M.; Playford, P.E.; Steffensen, C.K.; Andres, M.S.; Suosaari, G.V.; Milano, G.R.; Eberli, G.P. Stromatolite Provinces of Hamelin Pool: Physiographic Controls on Stromatolites and Associated Lithofacies. *J. Sediment. Res.* **2019**, *89*, 207–226. [[CrossRef](#)]
13. Ginsburg, R.N. Controversies about Stromatolites: Vices and Virtues. In *Symposium Controversies in Modern Geology*; Academic Press: London, UK, 1991; pp. 25–36.
14. Kaźmierczak, J.; Coleman, M.L.; Gruszczynski, M.; Kempe, S. Cyanobacterial Key to the Genesis of Micritic and Peloidal Limestones in Ancient Seas. *Acta Palaeontol. Pol.* **1996**, *41*, 319–338.
15. Awramik, S.M.; Riding, R. Role of Algal Eukaryotes in Subtidal Columnar Stromatolite Formation. *Proc. Natl. Acad. Sci. USA* **1988**, *85*, 1327–1329. [[CrossRef](#)]
16. Browne, K.M. *Modern Marine Stromatolitic Structures: The Sediment Dilemma BT—STROMATOLITES: Interaction of Microbes with Sediments*; Tewari, V., Seckbach, J., Eds.; Springer: Dordrecht, The Netherlands, 2011; pp. 291–312. ISBN 978-94-007-0397-1.
17. Jahnert, R.J.; Collins, L.B. Characteristics, Distribution and Morphogenesis of Subtidal Microbial Systems in Shark Bay, Australia. *Mar. Geol.* **2012**, *303–306*, 115–136. [[CrossRef](#)]
18. Hagan, P.D. Internal Fabrics and Microbial Precipitation in the Stromatolites of Hamelin Pool, Western Australia. Ph.D. Thesis, University of Miami, Miami, FL, USA, 2015.
19. Goh, F.; Allen, M.A.; Leuko, S.; Kawaguchi, T.; Decho, A.W.; Burns, B.P.; Neilan, B.A. Determining the Specific Microbial Populations and Their Spatial Distribution within the Stromatolite Ecosystem of Shark Bay. *ISME J.* **2009**, *3*, 383–396. [[CrossRef](#)] [[PubMed](#)]
20. Hoffman, P. Shallow and Deepwater Stromatolites in Lower Proterozoic Platform-to-Basin Facies Change, Great Slave Lake, Canada. *AAPG Bull.* **1974**, *58*, 856–867. [[CrossRef](#)]
21. Kazmierczak, J.; Kempe, S. Genuine Modern Analogues of Precambrian Stromatolites from Caldera Lakes of Niuafu’ou Island, Tonga. *Naturwissenschaften* **2006**, *93*, 119–126. [[CrossRef](#)] [[PubMed](#)]
22. Burns, B.P.; Anitori, R.; Butterworth, P.; Henneberger, R.; Goh, F.; Allen, M.A.; Ibañez-Peral, R.; Bergquist, P.L.; Walter, M.R.; Neilan, B.A. Modern Analogues and the Early History of Microbial Life. *Precambrian Res.* **2009**, *173*, 10–18. [[CrossRef](#)]
23. Playford, P.E.; Cockbain, A.E.; Berry, P.F.; Roberts, A.P.; Haines, P.W.; Brooke, B.P. *Geology of Shark Bay*; Geological Survey of Western Australia: Perth, Australia, 2013; ISBN 9781741685039.
24. Logan, B.W.; Hoffman, P.; Gebelein, C.D. Algal Mats, Cryptalgal Fabrics, and Structures, Hamelin Pool, Western Australia. In *Memoir 22: Evolution and Diagenesis of Quaternary Carbonate Sequences, Shark Bay, Western Australia*; American Association of Petroleum Geologists (AAPG): Tulsa, OK, USA, 1974; pp. 140–194.
25. Playford, P.E. *Geology of the Shark Bay area, Western Australia*; Geological Survey of Western Australia: Perth, Australia, 1990.
26. BBablonia, J.; Conesa, A.; Casaburi, G.; Pereira, C.; Louyakis, A.S.; Reid, R.P.; Foster, J.S. Comparative metagenomics provides insight into the ecosystem functioning of the Shark Bay Stromatolites, Western Australia. *Front. Microbiol.* **2018**, *9*, 1359. [[CrossRef](#)]
27. Golubic, S.; Hofmann, H.J. Comparison of Holocene and Mid-Precambrian Entophysalidaceae (Cyanophyta) in Stromatolitic Algal Mats: Cell Division and Degradation. *J. Paleontol.* **1976**, *50*, 1074–1082.
28. Golubic, S.; Abed, R.M.M. Entophysalis Mats as Environmental Regulators. In *Microbial Mats*; Seckbach, J., Oren, A., Eds.; Springer: Dordrecht, The Netherlands, 2010; pp. 237–251. ISBN 9789048137992.
29. Playford, P.E.; Cockbain, A.E. Modern Algal Stromatolites at Hamelin Pool, A Hypersaline Barred Basin in Shark Bay, Western Australia. In *Stromatolites*; Walter, M.R.B.T.-D., Ed.; Elsevier: Amsterdam, The Netherlands, 1976; Volume 20, pp. 389–411. ISBN 0070-4571.
30. Nye, O.B.; Dean, D.A.; Hinds, R.W. Improved Thin Section Techniques for Fossil and Recent Organisms Published by: SEPM Society for Sedimentary Geology Stable. *J. Paleontol.* **1972**, *46*, 271–275.
31. Stolz, J.F.; Reid, R.P.; Visscher, P.T.; Decho, A.W.; Norman, R.S.; Aspden, R.J.; Bowlin, E.M.; Franks, J.; Foster, J.S.; Paterson, D.M.; et al. *The Microbial Communities of the Modern Marine Stromatolites at Highborne Cay, Bahamas*; National Museum Of Natural History Smithsonian Institution: Washington, DC, USA, 2009; pp. 1–29.
32. Friedman, G.M. Classification of sediments and sedimentary rocks. In *Encyclopedia of Sediments and Sedimentary Rocks*; Middleton, G.V., Church, M.J., Coniglio, M., Hardie, L.A., Longstaffe, F.J., Eds.; Springer Netherlands: Dordrecht, The Netherlands, 1978; pp. 127–136. ISBN 978-1-4020-3609-5.
33. Folk, R.L. Practical Petrographic Classification of Limestones1. *Am. Assoc. Pet. Geol. Bull.* **1959**, *43*, 1–38. [[CrossRef](#)]
34. Bontognali, T.R.R.; Vasconcelos, C.; Warthmann, R.J.; Dupraz, C.; Bernasconi, S.M.; McKenzie, J.A. Microbes Produce Nanobacteria-like Structures, Avoiding Cell Entombment. *Geology* **2008**, *36*, 663–666. [[CrossRef](#)]
35. Weiner, S.; Levi-Kalisman, Y.; Raz, S.; Addadi, L. Biologically Formed Amorphous Calcium Carbonate. *Connect. Tissue Res.* **2003**, *44*, 214–218. [[CrossRef](#)] [[PubMed](#)]
36. Walker, J.M.; Marzec, B.; Nudelman, F. Solid-State Transformation of Amorphous Calcium Carbonate to Aragonite Captured by CryoTEM. *Angew. Chemie Int. Ed.* **2017**, *56*, 11740–11743. [[CrossRef](#)] [[PubMed](#)]
37. Enyedi, N.T.; Makk, J.; Kótai, L.; Berényi, B.; Klébert, S.; Sebestyén, Z.; Molnár, Z.; Borsodi, A.K.; Leél-Óssy, S.; Demény, A.; et al. Cave Bacteria-Induced Amorphous Calcium Carbonate Formation. *Sci. Rep.* **2020**, *10*, 8696. [[CrossRef](#)] [[PubMed](#)]
38. Kazmierczak, J.; Kremer, B.; Racki, G. Late Devonian Marine Anoxia Challenged by Benthic Cyanobacterial Mats. *Geobiology* **2012**, *10*, 371–383. [[CrossRef](#)]

39. Baumgartner, R.J.; Van Kranendonk, M.J.; Wacey, D.; Fiorentini, M.L.; Saunders, M.; Caruso, S.; Pages, A.; Homann, M.; Guagliardo, P. Nano-Porous Pyrite and Organic Matter in 3.5-Billion-Year-Old Stromatolites Record Primordial Life. *Geology* **2019**, *47*, 1039–1043. [[CrossRef](#)]
40. Dupraz, C.; Visscher, P.T. Microbial Lithification in Marine Stromatolites and Hypersaline Mats. *Trends Microbiol.* **2005**, *13*, 429–438. [[CrossRef](#)]
41. Braissant, O.; Decho, A.W.; Dupraz, C.; Glunk, C.; Przekop, K.M.; Visscher, P.T. Exopolymeric Substances of Sulfate-Reducing Bacteria: Interactions with Calcium at Alkaline PH and Implication for Formation of Carbonate Minerals. *Geobiology* **2007**, *5*, 401–411. [[CrossRef](#)]
42. Gallagher, K.L.; Kading, T.J.; Braissant, O.; Dupraz, C.; Visscher, P.T. Inside the Alkalinity Engine: The Role of Electron Donors in the Organomineralization Potential of Sulfate-Reducing Bacteria. *Geobiology* **2012**, *10*, 518–530. [[CrossRef](#)]
43. Hagan, G.M.; Logan, B.W. *Development of Carbonate Banks and Hypersaline Basins, Shark Bay, Western Australia*; American Association of Petroleum Geologists (AAPG): Tulsa, OK, USA, 1974.
44. Jahnert, R.J.; Collins, L.B. Controls on Microbial Activity and Tidal Flat Evolution in Shark Bay, Western Australia. *Sedimentology* **2013**, *60*, 1071–1099. [[CrossRef](#)]
45. Balci, N.; Demirel, C.; Akcer ÖN, S.; Gültekin, A.H.; Kurt, M.A. Evaluating Abiotic and Microbial Factors on Carbonate Precipitation in Lake Acigöl, a Hypersaline Lake in Southwestern Turkey. *Quat. Int.* **2018**, *486*, 116–128. [[CrossRef](#)]
46. Golubic, S. Stromatolites, Fossil and Recent: A Case History. In *Biomining and Biological Metal Accumulation*; Westbroek, P., de Jong, E.W., Eds.; D. Reidel Publishing Company: Dordrecht, The Netherlands, 1983; pp. 313–326.
47. Golubic, S. Microbial Mats and Modern Stromatolites in Shark Bay, Western Australia. In *Planet Ecology*; Van Nostrand Reinhold Co.: New York, NY, USA, 1985; pp. 3–16.
48. Jahnert, R.J.; Collins, L.B. Significance of Subtidal Microbial Deposits in Shark Bay, Australia. *Mar. Geol.* **2011**, *286*, 106–111. [[CrossRef](#)]
49. Riding, R. Calcareous Algae and Stromatolites. In *Calcareous Algae and Stromatolites*; Riding, R., Ed.; Springer-Verlag: Berlin, Germany, 1991; pp. 21–51. ISBN 9783642523359.
50. Horodyski, R.J.; Vonder Haar, S.P. Recent Calcareous Stromatolites from Laguna Mormona (Baja California) Mexico. *J. Sediment. Petrol.* **1975**, *45*, 894–906. [[CrossRef](#)]
51. Allen, C.C.; Albert, F.G.; Chafetz, H.S.; Combie, J.; Graham, C.R.; Kieft, T.L.; Kivett, S.J.; McKay, D.S.; Steele, A.; Taunton, A.E.; et al. Microscopic Physical Biomarkers in Carbonate Hot Springs: Implications in the Search for Life on Mars. *Icarus* **2000**, *147*, 49–67. [[CrossRef](#)] [[PubMed](#)]
52. Kazmierczak, J.; Altermann, W.; Kremer, B.; Kempe, S.; Eriksson, P.G. Mass Occurrence of Benthic Coccoid Cyanobacteria and Their Role in the Production of Neoproterozoic Carbonates of South Africa. *Precambrian Res.* **2009**, *173*, 79–92. [[CrossRef](#)]
53. Melim, L.A.; Northup, D.E.; Boston, P.J.; Spilde, M.N. Preservation of Fossil Microbes and Biofilm in Cave Pool Carbonates and Comparison to Other Microbial Carbonate Environments. *Palaios* **2016**, *31*, 177–189. [[CrossRef](#)]
54. Awramik, S.M. Ancient Stromatolites and Microbial Mats. In *Microbial Mats: Stromatolites*; Cohen, Y., Castenholz, R.W., Halvorson, H.O., Eds.; Alan, R. Liss Inc.: New York, NY, USA, 1984; pp. 1–21.
55. Kennard, J.; James, N.P. Thrombolites and Stromatolites: Two Distinct Types of Microbial Structures. *Palaios* **1986**, *1*, 492–503. [[CrossRef](#)]
56. Sumner, D.Y. Microbial vs Environmental Influences on the Morphology of Late Archean Fenestrate Microbialites. In *Microbial Sediments*; Riding, R.E., Awramik, S.M., Eds.; Springer: Berlin/Heidelberg, Germany, 2000; pp. 307–314. ISBN 978-3-662-04036-2.
57. Suarez-Gonzalez, P.; Benito, M.I.; Quijada, I.E.E.; Mas, R.; Campos-Soto, S. ‘Trapping and Binding’: A Review of the Factors Controlling the Development of Fossil Agglutinated Microbialites and Their Distribution in Space and Time. *Earth-Sci. Rev.* **2019**, *194*, 182–215. [[CrossRef](#)]
58. Sugitani, K.; Mimura, K.; Nagaoka, T.; Lepot, K.; Takeuchi, M. Microfossil Assemblage from the 3400Ma Strelley Pool Formation in the Pilbara Craton, Western Australia: Results Form a New Locality. *Precambrian Res.* **2013**, *226*, 59–74. [[CrossRef](#)]
59. Gong, Y. Sedimentary Fabrics for Thrombolite Bioherm in Cambrian Zhangxia Formation in the Western Part of Shandong Province. *IOP Conf. Ser. Earth Environ. Sci.* **2021**, *781*, 052006. [[CrossRef](#)]
60. Bahniuk, A.M.; Anjos, S.; França, A.B.; Matsuda, N.; Eiler, J.; Mckenzie, J.A.; Vasconcelos, C. Development of Microbial Carbonates in the Lower Cretaceous Codó Formation (North-East Brazil): Implications for Interpretation of Microbialite Facies Associations and Palaeoenvironmental Conditions. *Sedimentology* **2015**, *62*, 155–181. [[CrossRef](#)]
61. Warren, L.V.; Varejão, F.G.; Quaglio, F.; Simões, M.G.; Fürsich, F.T.; Poiré, D.G.; Catto, B.; Assine, M.L. Stromatolites from the Aptian Crato Formation, a Hypersaline Lake System in the Araripe Basin, Northeastern Brazil. *Facies* **2017**, *63*, 3. [[CrossRef](#)]
62. Backus, D.H.; Johnson, M.E. Stromatolitic Mats from an Uplifted Pleistocene Lagoon at Punta Chivato on the Gulf of California (Mexico). *Palaios* **2014**, *29*, 460–466. [[CrossRef](#)]
63. Caudwell, C.; Lang, J.; Pascal, A. Lamination of Swampy-Rivulets Rivularia Haematites Stromatolites in a Temperate Climate. *Sediment. Geol.* **2001**, *143*, 125–147. [[CrossRef](#)]
64. Lundberg, J.; McFarlane, D.A. Subaerial Freshwater Phosphatic Stromatolites in Deer Cave, Sarawak—A Unique Geobiological Cave Formation. *Geomorphology* **2011**, *128*, 57–72. [[CrossRef](#)]

65. Shirokova, L.S.; Mavromatis, V.; Bundeleva, I.A.; Pokrovsky, O.S.; Bénézech, P.; Gérard, E.; Pearce, C.R.; Oelkers, E.H. Using Mg Isotopes to Trace Cyanobacterially Mediated Magnesium Carbonate Precipitation in Alkaline Lakes. *Aquat. Geochemistry* **2013**, *19*, 1–24. [[CrossRef](#)]
66. Sanz-Montero, M.E.; Cabestrero, Ó.; Sánchez-Román, M. Microbial Mg-Rich Carbonates in an Extreme Alkaline Lake (Las Eras, Central Spain). *Front. Microbiol.* **2019**, *10*, 148. [[CrossRef](#)]
67. Balci, N.; Gunes, Y.; Kaiser, J.; On, S.A.; Eris, K.; Garczynski, B.; Horgan, B.H.N. Biotic and Abiotic Imprints on Mg-Rich Stromatolites: Lessons from Lake Salda, SW Turkey. *Geomicrobiol. J.* **2020**, *37*, 401–425. [[CrossRef](#)]
68. Popall, R.M.; Bolhuis, H.; Muyzer, G.; Sánchez-Román, M. Stromatolites as Biosignatures of Atmospheric Oxygenation: Carbonate Biomineralization and UV-C Resilience in a *Geitlerinema* sp.—Dominated Culture. *Front. Microbiol.* **2020**, *11*, 948. [[CrossRef](#)]